

The mantle isotopic printer.

Basic mantle plume geochemistry for seismologists and geodynamicists

Michele Lustrino^{1,2} and Don L. Anderson³

1 = Dipartimento di Scienze della Terra, Università degli Studi di Roma La Sapienza, P.le A. Moro, 5, 00185 Roma

2 = CNR Istituto di Geologia Ambientale e Geoingegneria (IGAG) c/o Dipartimento di Scienze della Terra, Università degli Studi di Roma La Sapienza, P.le A. Moro, 5, 00185 Roma

3 = Seismological Laboratory, California Institute of Technology, Pasadena, CA, 91125, USA

* Corresponding author: michele.lustrino@uniroma1.it

"Sunt aliquot quoque res quarum unam dicere causam non satis est, verum pluris, unde una tamen sit"
(There are phenomena for which it is not sufficient to infer a single origin, but it is necessary to propose several, among which, however, only one is true).

Lucretius. De Rerum Natura (VI, 703-705)

17 Abstract

18 High-temperature geochemistry combined with igneous petrology is an essential tool to infer the
19 conditions of magma generation and evolution in the Earth's interior. During the last thirty years a
20 large number of geochemical models of the Earth, essentially inferred from the isotopic
21 composition of basaltic rocks, have been proposed. These geochemical models have paid little
22 attention to basic physics concepts, broad-band seismology, or geological evidence, with the effect
23 of producing results that are constrained more by assumptions than by data or first principles. This
24 may not be evident to seismologists and geodynamicists.

25 A common view in igneous petrology, seismology and mantle modelling is that isotope
26 geochemistry (e.g., the Rb-Sr, Sm-Nd, U-Th-Pb, U-Th-He, Re-Os, Lu-Hf, and other more complex
27 systems) has the power to identify physical regions in the mantle, their depths, their rheological
28 behaviour and the thermal conditions of magma generation. We demonstrate the fallacy of this
29 approach and the model-dependent conclusions that emerge from unconstrained or poorly
30 constrained geochemical models that do not consider physics, seismology (other than teleseismic
31 travel time tomography and particularly compelling colored mantle cross sections) and geology.

32 Our view may be compared with computer printers. These can reproduce the entire range of colors
33 using a limited number of basic colors (black, magenta, yellow, and cyan). Similarly, the isotopic
34 composition of oceanic basalts and nearly all their primitive continental counterparts can be
35 expressed in terms of a few mantle end-members. The four most important (actually "most
36 extreme", since some are extraordinarily rare) mantle end-members identified by isotope
37 geochemists are DMM or DUM [Depleted MORB (mid-ocean-ridge basalt) Mantle or Depleted
38 Upper Mantle], HiMu (High-Mu, where $\mu = \mu = {}^{238}\text{U}/{}^{204}\text{Pb}$), EMI and EMII (Enriched Mantle
39 type I and type II). Other mantle end-members, or components, have been proposed in the
40 geochemical literature (e.g., PHeM, FoZo, LVC, PreMa, EMIII, CMR, LoMu, and C) but these can
41 be considered to be less extreme components or mixtures in the geochemical mantle zoo.

42 Assuming the existence of these extreme "colors" in the mantle isotopic printer, the only matter
43 for debate is their location in the Earth's interior. At least three need long-time insulation from
44 convection-driven homogenization or mixing processes. In other words, it needs to be defined
45 where these extreme isotopic end-members are located. In our view, no geochemical, geological,
46 geophysical and physical arguments require the derivation of any basalt or magma from the deep
47 mantle. Arguments to the contrary are assumption-based. The HiMu, EMI and EMII end-members

48 can be entirely located in the shallow non-convecting volume of the mantle, while the fourth, which
49 is by far the more abundant volumetrically, (DMM or DUM) can reside in the Transition Zone.

50 This view is inverted compared with current canonical geochemical views of the Earth's mantle,
51 where the shallowest portions are assumed to be DMM-like (ambient mantle) and the EMI-EMII-
52 HiMu end-members are assumed to be isolated, located in the deep mantle, and associated with
53 thermal anomalies. We argue that the ancient, depleted signatures of DMM imply long-term
54 isolation from recycling and crustal contamination while the enriched components are not free of
55 contamination by shallow materials and can therefore be shallow.

56

57 **1. Introduction**

58 Despite nearly half a century of detailed study, a consensus on the thermal state and chemical
59 composition of the Earth's interior has not yet been reached. The current canonical models of
60 geochemistry evolved essentially independently of classical physics, thermodynamics- and
61 seismology-based models. Secondary issues are not well resolved, and the gross features of the
62 Earth are the subject of debate. Among these, the geothermal gradient of the deep Earth and the
63 chemical vs. thermal causes for absolute and relative changes in seismic wave speed with depth are
64 debated (e.g., Anderson, 2007, 2011, 2013; Foulger et al., 2013). To constrain the basic features of
65 the Earth's structure, it is essential to understand the dynamics of our planet in terms of petrogenetic
66 processes.

67 The origin of igneous activity in intra-plate settings remains far from fully understood. At one
68 time it was considered to be a solved problem. In one view cracks and fractures tapped existing
69 melts in the low-velocity zone under the fast-moving plates (the 'jet-stream' of Wilson, 1963), but
70 other views were that deep sources were required for the existence of island chains and melts in the
71 shallow mantle away from plate boundaries required deep, hot upwellings (e.g., Morgan, 1971,
72 1972). Recent high-resolution global marine gravity models of the oceanic basins reveal a wealth of
73 buried tectonic structures many of which may be of igneous origin (Sandwell et al., 2014). These
74 features obscure the early defined oceanic chain trends allowing the hypothesis of more widespread
75 igneous activity, possibly related to the close-to-solidus condition of the shallow mantle.

76 While a general consensus has been reached on the causes of partial melting of the shallow mantle
77 beneath oceanic ridges and along subduction zones, the origin of intra-plate igneous activity is still
78 the subject of two different models based on opposite philosophical views.

79

80 Plume-based model

81 The first model argues that in order to have melts in areas away from plate boundaries it is
82 necessary to invoke thermal anomalies in the form of solid, deep mantle upwellings called mantle
83 plumes. In this model, the buoyancy of mantle plumes is related to their derivation from the
84 lowermost mantle (the seismic D" region) and its superadiabatic gradient. Adiabaticity is related to
85 relaxation as pressure decreases. The assumed adiabatic gradient for solid mantle rocks is ~ 0.4-0.6
86 °C/km, while more compressible liquids are characterized by higher adiabatic gradients around 1
87 °C/km (McKenzie and Bickle, 1988; Anderson, 2007). A superadiabatic gradient refers to
88 temperature decrease (with decreasing pressure) >0.6 °C/km. Superadiabatic gradients are
89 necessary for convection.

90 The mantle plume model requires important assumptions: 1) a chemically homogeneous upper
91 mantle characterized by a restitic (refractory) composition (harzburgitic to low-clinopyroxene
92 lherzolite) unable to produce large amounts of basaltic melts (e.g., Cadoux et al., 2007; Pfander et
93 al., 2012; Hart, 2014); 2) a maximum temperature at the base of the seismic LID (the outermost
94 shell of Earth characterized by an increase of seismic waves with depth) of ~1300 °C (e.g.,
95 McKenzie and Bickle, 1988; Fullea et al., 2009); 3) low-T and isothermal conditions for the entire
96 sub-lithospheric mantle down to the TZ (assumed in some mantle plume numerical modelling), the
97 mantle volume extending between the olivine/wadsleyite polymorph transition (~410 km) and the
98 ringwoodite/bridgmanite transition (the first is an olivine polymorph, while the second is Mg-Fe
99 silicate perovskite), occurring at ~660-670 km (e.g., Sobolev et al., 2011); 4) the presence of a
100 primitive (i.e., never before, or only poorly melted or degassed) lower mantle resembling CI-
101 chondrites (i.e., the most primitive compositions in the solar system). An alternative model relates
102 the gas-rich D" region to accumulation of noble-gas-rich recycled hybrid pyroxenites and subducted
103 eclogites (e.g., Davies, 2011); 5) an overall adiabatic geotherm for the bulk of the mantle (from
104 ~250 to ~2800 km depth; e.g., Glisovic and Forte, 2014) and 6) high "excess" potential
105 temperatures (T_p) of plume mantle (hypothesized on the basis of geochemical arguments relating to
106 magma compositions; Putirka 2005; Herzberg, 2011), where T_p is the temperature of a solid rock
107 brought to the surface adiabatically, resulting in a decrease of ~0.6 °C/km; 7) negative v_p and v_s
108 seismic anomalies imply temperature excess (Montelli et al., 2004; White, 2010; Faccenna and
109 Becker, 2010).

110 On these grounds, partial melting in the shallow intra-plate mantle is considered improbable (at
111 least to high degrees) given that this volume is assumed to be too cold and too refractory.
112 Consequentially, the source of intra-plate magma was considered to be related to solid mantle
113 upwellings from depths as great as 2800-2900 km (e.g., Morgan, 1971, 1972; White, 2010, Li et al.,
114 2014). The requirement of a single convection system, involving the entire sub-lithospheric mantle
115 is a conundrum in this model.

116 High T_p of mantle plumes cannot be directly measured and are assumed on the basis of the high
117 Fo (Forsterite) content [$Fo = Mg/(Mg+Fe)$] of olivines found in basaltic melts. Olivines are
118 common minerals in equilibrium with high-temperature melts, whose composition is essentially
119 represented by the Fo content. During peridotite partial melting, Fe in olivines (and all other
120 common silicate minerals present in the mantle, orthopyroxene, clinopyroxene and garnet) is
121 preferentially partitioned into the melt compared to Mg. At the same time, when olivine crystallizes
122 in a cooling basaltic magma, it preferentially hosts Mg compared to Fe. This means that the
123 maximum Fo content in an olivine crystallizing from a primitive basaltic melt (typically 0.75-0.85)
124 is always lower than the Fo content in the peridotite (typically 0.88-0.93).

125 In order to have a Fo-rich olivine in a basaltic magma, a lot of Mg must be available in the
126 crystallizing melt. According to the common view (e.g., Herzberg, 2011), in order to have a lot of
127 Mg in a basaltic melt very high temperatures are required (because, otherwise, MgO prefers
128 remaining into the solid residua). The typical rationale is, then, high-Fo olivine in a melt = high
129 MgO in the crystallizing magma = high T to generate such magma = high T_p of its mantle source to
130 extract as much MgO as possible from the peridotite. As we show below, high temperature regimes
131 are only one of the possible ways to explain a high MgO content in a melt.

132

133 Shallow Earth dynamics-based model

134 The second model considers the presence of chemical, rather than thermal, anomalies to explain
135 partial melting processes and seismic wave speed heterogeneities. Olivine-poor lithologies
136 characterized by low solidus temperature can melt under “normal” conditions, without requiring a
137 thermal anomaly. In other words, in order to have partial melt production in the mantle it is
138 necessary to have high homologous temperature (the ratio of the mantle absolute
139 temperature/solidus temperature) not high absolute temperature (e.g., Anderson, 2007; Foulger,
140 2010). In this view the upper mantle is completely different from that hypothesized in the previous

141 model. It is a chemically, mineralogically, thermally and rheologically heterogeneous *melange*, a
142 sort of a sheared baklava, marble-cake or plum-pudding system. Here, volumetrically predominant
143 olivine-rich lithologies (harzburgitic to lherzolitic matrix) are associated with olivine-poor to
144 olivine-free, garnet±phlogopite±amphibole±pyroxene-rich lithologies, representing subducted
145 lithologies, frozen basaltic melts, or the reaction products of melts derived from carbonated-
146 hydrated subducted lithologies within the peridotitic matrix (e.g., Niu et al., 2011; Mallik and
147 Dasgupta, 2014; Pilet, in press).

148 Melts characterized by high bulk MgO content are commonly associated with high MgO-olivines,
149 with forsterite as high as 95%. A Fo content >95% means that 95 atoms out of 100, excluding Si
150 and O and other minor bivalent constituents, are Mg, the remaining being Fe²⁺. These high-MgO
151 melts and minerals are found also in very low volume continental Ca-Na-Al-Ti-poor ultrapotassic
152 subduction-related rocks, which are certainly unrelated to mantle plumes (e.g., Prelevic and Foley,
153 2007). High MgO content in magma and associated olivine, coupled with low content of “basaltic”
154 components (i.e., elements that typically partition into the melt during mantle anatexis) indicate that
155 the source material was depleted [i.e., was involved in former partial melt extraction event(s)]. This
156 rules out any connection between the MgO content (in melt and olivine) and absolute temperature
157 of formation (e.g., Keiding et al., 2011), but rather associates MgO-rich melts and Fo-rich olivines
158 with depleted sources. Also the Fo-rich olivines and the high MgO content of picrites and other
159 MgO-rich volcanic rocks (komatiites and meimechites, all rocks with >12 wt% MgO and >52 wt%
160 SiO₂) could be due at least partially, if not entirely, to the presence of MgO-rich cumulitic olivine or
161 to ultra-depleted compositions, as for example recorded in Gorgona Island komatiite melt inclusions
162 (Arndt et al., 1997).

163 Recent geophysical and petrological considerations (e.g., Kawakatsu et al., 2009; Anderson,
164 2011, 2013) have modified the shallow mantle model for intra-plate volcanism, hypothesizing the
165 presence of diffuse melt lamellae in the Low Velocity Zone, a volume known from seismology
166 since the 1960s (Gutenberg, 1959; Fig. 1b). V_p and V_s wave speeds are consistent with a ~100-150
167 km-thick layer at depths of 200 km ± 50 km containing small melt pods. These melt lamellae,
168 aligned in a peridotitic matrix, are not usually in physical contact with each other and, therefore,
169 cannot easily escape to the surface.

170 The solidus temperature of a natural system is the temperature at which the first melt is produced.
171 Natural systems can experience partial melting if temperature increases. This is the basis on which

172 the mantle plume theory rests. A temperature excess is expected to be associated with upwelling of
173 solid diapirs from the base of the lowermost mantle. Alternatively, melts can be produced under
174 “normal” conditions (i.e., without invoking absolute temperature excess) if H and/or C is available.
175 Hydrogen can break the bonding oxygens connecting the SiO_4^{4-} tetrahedrons of mantle minerals and
176 eventually lead to strong viscosity reduction and partial melting.

177 The maximum amounts of H_2O that can be stored in pyroxenes, olivine and garnet in the shallow
178 mantle (i.e. at depths <14 GPa, corresponding to 410 km depth) does not exceed 0.1-0.2 wt%.
179 Higher amounts of H_2O can be stored in the upper mantle in so-called “exotic” mantle silicates such
180 as mica and amphibole, minerals that can host up to ~3 wt%. Rarely up to 10-12 wt% can be stored
181 in other silicates such as antigorite, chlorite and lawsonite (Schmidt and Poli, 2014; Vitale
182 Brovarone and Beyssac, 2014). The presence of these minerals, however, is conditioned to the
183 presence of light elements such as K (for the phlogopite mica) and Ca (for pargasite amphibole and
184 lawsonite) and low temperature regimes in general. With increasing pressure, olivine polymorphs
185 (wadsleyite and ringwoodite) become more prone to host water, and up to 2.5 wt% H_2O can be
186 forced into their lattices (Pearson et al., 2014).

187 In contrast with hydrogen, carbon is a completely incompatible element in typical silicate mantle
188 minerals. This means that, even at small levels, it forms its own solid phases (e.g., graphite,
189 diamond, carbonates, iron carbides) or partitions into melts (e.g., Hirschmann and Dasgupta, 2009).

190 The water storage capacity of a mantle rock is the weighted sum of the maximum amount of H_2O
191 that can be stored in the minerals. This capacity is variable and generally low – no more than 0.4-
192 0.5 wt% at depths <3 GPa, reducing to <0.1 wt% in the pressure range 3-12 GPa (Green et al.,
193 2010). A water content below the maximum storage capacity means that no free water is available,
194 all the H_2O being stored in silicate minerals. Under these circumstances the effect of the water in
195 breaking the bonding oxygens is weak. Only if vapour-saturated conditions are reached (i.e., the
196 amount of water exceeds the maximum water storage capacity of the mantle rocks) is partial
197 melting encouraged, as the solidus temperature abruptly drops. The difference in solidus
198 temperature between volatile-free and vapour-saturated conditions can be as high as 500 °C at 4
199 GPa (e.g., Litasov et al., 2011).

200 The most common hydrous phase in the mantle (pargasitic amphibole) is stable at depths lower
201 than ~100 km. The other hydrous phases (the so-called alphabetic phases, synthesized in the

202 laboratory only, like Phase A, B, E, Super E, 10 Å, and so on) stable only at temperatures much
203 lower than “normal” geotherms (e.g., Litasov and Ohtani, 2003; Schmidt and Poli, 2014).

204 The presence of stable carbonate minerals (essentially in the form of dolomite [CaMg(CO₃)₂] to
205 magnesite [MgCO₃]) contributes to lowering the solidus temperature of the peridotitic assemblage,
206 favouring melts with carbonatitic to carbonate-silicate compositions (e.g., Lee et al., 2000;
207 Gudfinnsson and Presnall, 2005; Keshav and Gudfinnsson, 2014). This happens because the solidus
208 temperature of carbonate minerals at mantle depths is several hundred degrees lower than for
209 volatile-free silicate minerals (with a $\Delta T > 500$ °C at 4 GPa).

210 The presence of melt may thus be related not to absolute temperature excesses but to small
211 amounts of CO₂ (easily prone to react with mantle silicates to produce Mg-Ca-Fe carbonates,
212 minerals characterized by low melting temperature), high water contents (above the water storage
213 capacity) or the absence of hydrous minerals at “normal” geotherm values. In other words, melting
214 can be present in conditions of high homologous temperature.

215

216 **2. How to understand the Earth’s interior**

217 Earth’s thermal profile.

218 As stated by White (2010), “*the plume hypothesis is essentially a physical one*”. Also Hofmann
219 (2014) underlines that “*most geochemical tracers carry no information about the specific mantle*
220 *depth being sampled*” and that “*geochemistry cannot prove mantle plumes*”, meaning that the
221 mantle plume concept is based on a hypothetical structural model of the Earth’s interior, and
222 geochemistry is an ancillary discipline serving to strengthen the model. Foulger et al. (2013)
223 highlighted the fundamental limitations of, and uncertainties in, seismic tomographic results. These
224 uncertainties include the difficulty of defining background models and obtaining absolute seismic
225 anomalies. These uncertainties derive from the variable chemical compositions and thermal states
226 of the upper mantle. In order to translate into temperature a seismic wave speed anomaly, it is
227 necessary to know the physical parameters of that volume (bulk and shear moduli, thermal
228 expansion and compressibility parameters, anisotropy, presence of volatiles, melts and exotic
229 phases, Fe-Mg ratios in the main minerals, grain-size, and so on). Only assuming *a priori* chemical,
230 mineralogical and lithological compositions may the tomographic results be interpreted in terms of
231 mantle temperature. Clearly, these parameters cannot be known everywhere for heterogeneous
232 systems like the upper mantle. Smith (in press) underlines that when anisotropy is taken into

233 consideration, the wave speed reduction interpreted as temperature anomalies in classical
234 tomographic images (assuming isotropic mantle structure) simply disappear.

235 Fluid dynamic simulations of the Earth's interior and geochemical arguments on basaltic
236 volcanism typically assume core temperatures maintained constant by the release of latent heat of
237 crystallization of the liquid core (e.g., Schuberth et al., 2009; Campbell and Griffiths, 2014;
238 Nakagawa and Tackley, 2014).

239 The classical seismological scheme of Earth's mantle involves four main regions (Regions B, C,
240 D' and D"; Fig. 1b), with the crust representing Region A. The uppermost ~200 km of the Earth
241 (Regions A and B) is characterized by a superadiabatic gradient, with rapid temperature increase
242 over a relatively small depth range, passing from temperatures near to zero to about 1300-1500 °C
243 at its base (Fig. 1).

244 The lower part of Region B (known as B'') is a thermal and shear boundary layer. The bulk of the
245 mantle (all but Region B) is usually assumed to be adiabatic down to the core-mantle boundary
246 layer at ~2700-2800 km. This cannot be the case for an internally heated or secularly cooling
247 mantle. The base of the lowermost mantle, Region D'' is characterized by another sharp increase of
248 temperature (superadiabatic gradient) estimated between 800 and 1300 °C (Jeanloz and Morris,
249 1986; Boehler et al., 1995; Campbell and Griffiths, 2014; Fig. 1b).

250 According to this classical view, the two most important thermal boundary layers of the Earth's
251 interior are the very shallow regions (which contain the lithosphere, LID, and plate – Regions A and
252 B'; see Anderson, 2011 for a review of the different meanings and implications of these terms) and
253 Region D'', located at ~2800-2900 km depth. The canonical view assumes, to resume, an adiabatic
254 geotherm for the bulk of the mantle, a superadiabatic D'' (caused by the strong heating from below),
255 a vigorous whole-mantle convection below Region B', a consequent chemical homogeneity, lack of
256 layering, no internal heating and no slabs to cool its interior (Figs. 1a and 1b). According to this
257 pot-on-the-stove view, the Earth's mantle is heated from below by a constant-temperature heat
258 source.

259 A corollary of fluid dynamic simulations is a self-compressed Earth heated by a constant
260 temperature core-mantle boundary triggering whole-mantle overturn, with limited obstruction, if
261 any, by the TZ. Hot, solid, but narrow mantle blobs are assumed to depart from the D'' layer,
262 moving through the entire mantle, and eventually melting when they reach shallow mantle depths
263 (Fig. 1b). Both early and recent modelling (e.g., Griffiths and Campbell, 1990; Farnetani and

264 Richards, 1994; Ballmer et al., 2013; Cloetingh et al., 2013; Bull et al., 2014; Li et al., 2014),
265 assume prescribed and constant temperatures, modes of convection, adiabaticity, and non-cooling
266 interfaces.

267 Alternatively, mantle convection could be caused by heat lost from the surface to space rather than
268 by heat released by the crystallizing liquid core. The differences are not subtle. In the former case,
269 surface cooling triggers convection, favouring delamination of cold portions of the shallow mantle
270 and passive upwelling in the mantle (e.g., Anderson and King, 2014; Anderson and Natland, 2014).
271 Moreover, the mantle cools the core, while in plume modelling and in canonical geodynamic and
272 geochemical models the core warms the mantle and convection is caused by heat excess at D".

273 The thick line indicated with (1) in Fig. 1b represents schematically the classically accepted
274 geotherm with two thermal boundary layers characterized by superadiabatic regimes, one close to
275 the surface (Regions A + B') and the other on top of the core (Region D"), with the bulk of the
276 mantle characterized by adiabatic geotherm (Regions B", C and D'). The thin line indicated with (2)
277 in the same figure is one of the possible geotherms (Schubert et al., 2009) characterized by
278 superadiabatic and subadiabatic trends and no adiabatic gradients. In the first scheme, with the
279 exclusion of D", maximum T_p is reached at the base of the lithosphere (~90-100 km in oceanic
280 basins), with T_p as high as ~1300 °C. Deeper mantle is hotter because it is self-compressed, but
281 when brought to a reference pressure (e.g., the Earth's surface) it is characterized by the same T_p
282 (~1300 °C) as the sub-lithospheric mantle. This temperature is considered the ambient mantle T_p , as
283 recorded by MORB (e.g., McKenzie and Bickle, 1988). The most important differences between the
284 two type of geotherms are: *a)* the maximum T_p of geotherm-1 is lower than that of geotherm-2; *b)*
285 the maximum T_p of geotherm-1 is reached at shallower depths than geotherm-2; *c)* after the thermal
286 bump at ~200 km the T_p in geotherm-2 decreases with depth while the T_p in geotherm-1 remains
287 constant for nearly the entire mantle; *d)* D" in geotherm-1 is characterized by higher T_p than the
288 entire mantle, while in geotherm-2 much of D" is characterized by lower T_p .

289 The dashed lines in Fig. 1b represent the adiabatic upwelling of two samples of the lowermost
290 mantle starting at temperatures compatible with geotherm-1 (star) and geotherm-2 (square). In the
291 first case (the classical mantle plume scheme) upwelling of solid mantle from D" is characterized by
292 higher T_p , recorded in high- T_p magma (inferred on the basis of high Mg/Fe ratios of melts and
293 associated olivines). In the second case (the fluid dynamically and internally heated compatible
294 model) upwelling of solid mantle from D" is characterized by lower T_p . The highest measurable T_p

295 in this case is associated with mantle corresponding to the LLAMA (*Laminated Lithology with*
296 *Aligned Melt Accumulations* or *Layer of Laterally Advecting Mass and Anisotropy*) region of
297 Anderson (2011), around 200-250 km depth, corresponding to the worldwide, well-defined Low
298 Velocity Zone (LVZ). What emerges is the (apparent) paradox that the deeper the source the colder
299 the Tp. The importance of this region (also corresponding to the old Perisphere of Anderson, 1995)
300 has been recently emphasized by Smith (in press).

301

302 Can geochemistry help?

303 The reason why plumes are still part of the canonical models of mantle geochemistry and
304 dynamics can be traced to insufficient interdisciplinary understanding, unquestioning acceptance of
305 the conclusions of others, and semantics. This is known in philosophy as incommensurability.
306 Seismologists are generally not fully aware of the assumptions underlying geochemical inferences
307 and simply accept the conclusions regarding primordial and undegassed mantles and the meaning of
308 concepts such as high $^3\text{He}/^4\text{He}$ or given Pb isotopic ratios. Likewise, geochemists are generally not
309 completely aware of the modelling assumptions in teleseismic travel time tomography and tend to
310 interpret color images of the mantle as thermometry. High-resolution seismic tomography has
311 confirmed that the mantle features used as evidence for active plumes are thousands of kilometres
312 in lateral extent and therefore probably neutral, passive and rising only slowly if at all. As a
313 consequence an alternative view (i.e., they are not thermal plumes nor active upwellings) has been
314 proposed (e.g., Anderson and Natland, 2014). It has also been confirmed that intra-plate volcanoes
315 such as Hawaii tap into a thick sheared shallow boundary layer that is sufficiently hot, fertile, large
316 and slowly moving to explain volcanic chains (Anderson, 2011; Smith, in press). Surprisingly, this
317 was originally proposed by Wilson (1963). This shallow layer is disrupted by 3D deep passive
318 upwellings that feed ridges and near-ridge hotspots.

319 The canonical paradigm of mantle dynamics and geochemistry includes whole-mantle convection
320 and whole-mantle plumes. It has been supported by three lines of evidence: radiogenic isotope
321 geochemistry, fluid dynamic simulations, and relative travel-time tomography. Each of these has
322 undergone paradigm shifts, even reversals, requiring reconsideration of the whole canonical model.
323 In the next sections we focus on those isotopic systematics most widely used in basalt petrogenesis.
324 We demonstrate how geochemical concepts do not require deep-mantle upwelling and,
325 consequentially, cannot be used as “smoking guns” for mantle plumes. Phrases such as “*the X value*

326 *of the Y isotopic systematic indicates the involvement of deep mantle plumes”* are simply incorrect.
327 Geochemistry does not have not the power to detect upwellings from the deep mantle and has only
328 limited power to infer the thermal state of the melt source.

329 330 **3. Principles of geochemistry applied to igneous petrology**

331 The upper thermal boundary layer, the upper 150-200 km of the Earth, is physically and
332 geochemically heterogeneous. This is confirmed by the mineralogy and geochemistry of mantle
333 xenoliths exhumed by alkali basaltic melts from the shallowest (typically 50-120 km depth; Nixon,
334 1987).

335 Despite this, the upper mantle is commonly assumed to be homogeneous, isotropic, chemically
336 depleted, olivine-rich and nearly H-C-free by geochemists and geophysical modellers (e.g., Cadoux
337 et al., 2007). In particular, the shallowest rigid portion of the mantle is considered to be stiff and
338 virtually incapable of producing basaltic melts unless at unrealistically high temperatures.
339 Sometimes the lithosphere is equated to the seismic LID or to the whole boundary layer. These
340 background hypotheses have important implications for interpreting isotopic “anomalies” in mantle-
341 derived materials and the travel-time anomalies of teleseismic waves. The LID and the lithosphere
342 are thin and this is one reason why geochemists look much deeper for magma sources.

343 In the standard geochemical model, the deep mantle is not involved in chemical differentiation. It
344 maintained a primordial chemical composition despite being continuously modified (enriched in
345 basaltic components) by arrival of subducted material that pierced the TZ. Several geochemical
346 models, based on unconstrained assumptions and forcing selected set of data to converge towards a
347 pre-fixed results, attempt to explain this paradox (e.g., Jackson et al., 2010, 2014; Davies, 2011).

348 Standard geochemical models require background lower mantle or liquid core thermal and
349 chemical inputs to explain the genesis of Ocean Island Basalts (OIB) and other supposed plume-
350 related volcanoes. In geochemistry, OIB is a generic term for intra-plate oceanic rocks characterised
351 by a large range of incompatible element content and a very large range of isotopic ratios. This
352 rock group comprises volumetrically predominant tholeiitic (i.e., Na-K-poor and with relatively
353 high Fe/Mg) and minor sodic alkaline basalts, along with very rare differentiated (i.e., silica-richer)
354 compositions such as trachytes and phonolites. In isotope geochemistry the term OIB is too vague
355 and several prefixes (e.g., HiMu, EMI, EMII and so on, which we explain later) are needed to
356 distinguish the various compositions.

357 In particular, isotope geochemistry is often considered by geochemists and geophysicists to be the
358 smoking gun for mantle plumes. We explain here why isotope geochemistry cannot be used as
359 evidence, much less definitive proof, for mantle plumes.

360

361 **The Rb-Sr isotope system.** This is the oldest and best studied isotopic system applied to igneous
362 petrogenesis (e.g., Faure and Powell, 1972). It is based on the natural decay (i.e., transformation) of
363 a radioactive isotope of Rubidium, ^{87}Rb (representing about 27.8% of the isotopes of Rb, the
364 remaining being the stable ^{85}Rb). Strontium has four stable isotopes, with atomic masses 84 (0.6%
365 of the Sr isotopes), 86 (9.9%), 87 (7%) and 88 (82.6%). The abundance ratios among the Sr isotopes
366 remain constant, with the exception of ^{87}Sr , which is continuously produced by ^{87}Rb decay.

367 The half-life of ^{87}Rb is 4.8×10^{10} yr (Table 1). Given that the age of the Earth is one tenth of this
368 half life, clearly the original ^{87}Rb at the time of the Earth's formation has been reduced only by a
369 small amount and the amount of ^{87}Sr has increased by only the same amount. The amount of ^{87}Sr
370 now measured in a rock (sedimentary, metamorphic or igneous) is the sum of the original ^{87}Sr plus
371 the amount produced after the decay of ^{87}Rb . Obviously, the higher the original content of Rb (and
372 hence ^{87}Rb) and the older a rock, the larger the amount of radiogenic ^{87}Sr produced.

373 During partial melting or fractional crystallization processes, the most important differentiation
374 processes in igneous geochemistry (except for the noble gases and stable isotopes), two isotopes of
375 the same element (e.g., ^{88}Rb and ^{87}Rb or ^{87}Sr and ^{86}Sr) are not fractionated and their ratios remain
376 unchanged. What may change is the elemental ratio of the parent and daughter isotope pairs. The
377 ionic radius of Rb (1.66 \AA , where $\text{\AA} = \text{Angstrom} = 1 \times 10^{-10} \text{ m} = 0.1 \text{ nm}$) is not much different from
378 that of K (1.52 \AA). Also the charge of Rb and K is the same (+1). These two characteristics render
379 Rb an element with a geochemical behaviour very similar to that of K. In other words, Rb can
380 substitute or replace K in minerals (e.g., K-feldspars or biotite). On the other hand, Sr (1.32 \AA ; +2
381 valence) shares much more geochemical affinity with Ca (1.14 \AA ; +2 valence). The Earth's mantle
382 has more Ca than K (Ca/K ratio of primitive mantle estimate being ~ 75 ; Lyubteskaya and
383 Korenaga, 2007).

384 During partial melting of a volatile-free peridotitic source, K behaves as a strongly incompatible
385 element (i.e., it has a strong tendency to prefer the melt phase), because there are no minerals in
386 which it can exist. Element incompatibility must always be expressed with respect to a given
387 mineral (or mineral assemblage) and a given melt composition. The compatibility of an element is

388 the ratio of its abundance in the mineral to its abundance in the liquid that is in equilibrium with it.
389 There is no element that is always “incompatible” (i.e., prefers the liquid phase) or “compatible”
390 (i.e., prefers the solid phase) under all conditions (e.g., Fedele et al., 2015).

391 Rubidium is incompatible in a peridotitic mantle. This means that, in the presence of melt, Rb is
392 preferentially partitioned there instead of remaining in the solid rock residuum. The same Rb is
393 compatible in a crystallizing rhyolitic melt (an alkali feldspar-rich volcanic rock). This means that
394 Rb will preferentially move into the crystallizing alkali feldspar as it precipitates.

395 Calcium behaves as a moderately incompatible element (because the only mineral in which it can
396 be stored, clinopyroxene, is among the first phases to melt). In a carbonated peridotite Ca continues
397 to behave as a moderately incompatible element, since carbonates are the first phases to melt, due to
398 their very low melting temperature compared with the other silicate minerals. The same holds in the
399 presence of garnet, a phase that can host large amounts of Ca at large depth in its Ca-majoritic form,
400 but that is among the first phases to melt. As a consequence, the K/Ca ratio (and also Rb/Sr) in a
401 partial melt of a peridotite (e.g., basalt) is higher than the K/Ca (or Rb/Sr) in the source. The higher
402 Rb/Sr, the higher $^{87}\text{Rb}/^{86}\text{Sr}$, where the numerator is a radioactive nuclide and the denominator is a
403 stable primordial isotope of Sr. With time, the higher $^{87}\text{Rb}/^{86}\text{Sr}$ evolves into higher $^{87}\text{Sr}/^{86}\text{Sr}$ because
404 ^{87}Rb slowly transforms to ^{87}Sr , while the ^{86}Sr content does not change.

405 The present-day $^{87}\text{Sr}/^{86}\text{Sr}$ isotopic ratio of the Bulk Silicate Earth (BSE, which represents the solid
406 Earth, excluding the core), is now known to be around 0.70445. This is the ratio the entire Earth
407 should have, assuming an original undifferentiated Earth $^{87}\text{Rb}/^{86}\text{Sr}$ ratio (~ 0.09 , present-day value)
408 and an initial $^{87}\text{Sr}/^{86}\text{Sr}$ of 0.69897 (Fig. 2). The initial $^{87}\text{Sr}/^{86}\text{Sr}$ of the Earth, called BABI (Basaltic
409 Achondrite Best Initial) is the Sr isotopic ratio of a basaltic achondrite meteorite with no Rb (and
410 thus no ^{87}Rb). This means that all the ^{87}Sr in that meteorite represents the primordial ^{87}Sr content of
411 the solar system. In other words, during its 4.56 Gyr life, the $^{87}\text{Sr}/^{86}\text{Sr}$ ratio of the Earth has
412 increased from 0.69897 (BABI) to 0.70445 (BSE), i.e., by only 0.00548, as result of ^{87}Rb decay.
413 Modern thermal ionization mass spectrometers can easily measure these very small ratio
414 differences, with the typical precision of $^{87}\text{Sr}/^{86}\text{Sr}$ ratios being $\pm 5 \times 10^{-6}$.

415 The present-day BSE value assumes an unchanged Rb/Sr isotopic ratio (Fig. 2). This is true if we
416 consider the entire Earth as a single system. But what happens if we consider the basalt-restite
417 mantle pair? (Restite is the residuum after extraction of partial melt.) Basalts are characterized by
418 Rb/Sr ratios higher than the original mantle and the restitic mantle. As a consequence, with ageing

419 we should expect in the basalt higher $^{87}\text{Sr}/^{86}\text{Sr}$, while the restitic mantle should be characterized by
420 lower $^{87}\text{Sr}/^{86}\text{Sr}$.

421 But how can the $^{87}\text{Sr}/^{86}\text{Sr}$ ratios in igneous rocks be used to constrain their origin? Let us assume
422 that at a given moment (e.g., 2 Gyr after its formation), the Earth experiences partial melting (Fig.
423 2; 1st partial melting event). This is a differentiation process, producing a partial melt which
424 eventually will solidify forming an igneous rock, leaving a restitic mantle. The first rock is
425 characterized by higher Rb/Sr, while the second shows lower Rb/Sr. After ~2.5 Gyr, the rock with
426 higher Rb/Sr (and thus higher $^{87}\text{Rb}/^{86}\text{Sr}$) will be characterized by a higher $^{87}\text{Sr}/^{86}\text{Sr}$ ratio compared
427 with the restitic source (Fig. 2). Both sources will have $^{87}\text{Sr}/^{86}\text{Sr}$ higher than at the moment of
428 partial melting, but the $^{87}\text{Sr}/^{86}\text{Sr}$ ratio of the igneous rock will be much higher than that of the
429 restite. The $^{87}\text{Sr}/^{86}\text{Sr}$ ratio of the restite (i.e., the mantle from which a given amount of partial melt
430 has been extracted in the past) is characterized by a $^{87}\text{Sr}/^{86}\text{Sr}$ ratio lower than the present-day BSE
431 $^{87}\text{Sr}/^{86}\text{Sr}$. The solidified partial melt can experience partial melting itself (2nd partial melting event
432 in Fig. 2). In this case, this process produces a new partial melt with higher Rb/Sr and a residual
433 source with lower Rb/Sr that will evolve towards different $^{87}\text{Sr}/^{86}\text{Sr}$ ratios (Fig. 2).

434 A second partial melting event of the first mantle residuum (3rd partial melting event in Fig. 2) will
435 produce a new melt and an even more depleted residuum. The final isotopic ratios of the different
436 partial melts and melt residua will depend on the initial $^{87}\text{Sr}/^{86}\text{Sr}$ ratios, the age of melt extraction,
437 the degree of Rb/Sr fractionation (essentially a function of source mineralogy and degree of
438 melting) and the ^{87}Rb half-life (Gast, 1960). In other words, a basalt (but also any other kind of
439 igneous rock) characterized by $^{87}\text{Sr}/^{86}\text{Sr}$ ratio lower than BSE is considered derived from a depleted
440 (i.e., non-primitive) mantle source. At very large degree melting, the liquid will have Rb/Sr ratios
441 converging to the original (primordial) values. Such large degrees of melting occurred only during
442 the accretion of the Earth.

443 What should the present day $^{87}\text{Sr}/^{86}\text{Sr}$ ratio of a basalt derived from a primitive mantle be (i.e., the
444 composition assumed for the lower mantle in some models)? Such a rock should have an $^{87}\text{Sr}/^{86}\text{Sr}$
445 ratio similar or very close to the BSE estimate. A conundrum for the classical mantle plume model
446 is that nearly all rocks whose origin is postulated to be related to plumes (e.g., HiMu-OIB) are
447 characterized by $^{87}\text{Sr}/^{86}\text{Sr}$ ratios <BSE, implying non-primitive mantle source compositions and
448 former partial melt extraction. Only a few OIB (EMI and EMII types) are characterized by $^{87}\text{Sr}/^{86}\text{Sr}$

449 ratios higher than BSE, but essentially none has the same isotopic composition as BSE (Stracke,
450 2012).

451 Igneous rocks are not all confined to $^{87}\text{Sr}/^{86}\text{Sr}$ ratios $<\text{BSE}$. An important part of the Earth
452 (essentially the upper crust) is characterized by sedimentary, metamorphic and igneous rocks with
453 $^{87}\text{Sr}/^{86}\text{Sr}$ ratios $>\text{BSE}$. This results from faster radiogenic growth of ^{87}Sr in rocks with $^{87}\text{Rb}/^{86}\text{Sr}$
454 ratios higher than the primordial Earth value. The average upper crust (as represented by the global
455 subducting sediment compilation of Plank, 2014) is old and characterized by high Rb (84 ppm;
456 compare this value with 0.46 ppm Rb of the primitive mantle), high Rb/Sr (0.27, compared with
457 0.03 of the primitive mantle), resulting in strongly radiogenic $^{87}\text{Sr}/^{86}\text{Sr}$ (0.7124; Plank, 2014).

458 Subduction is a process during which upper crust lithologies (or alteration products of them) are
459 recycled back to the mantle. During this process, rocks with high $^{87}\text{Sr}/^{86}\text{Sr}$ ratios are again mixed
460 with an upper mantle matrix characterized by $^{87}\text{Sr}/^{86}\text{Sr}$ ratios $<\text{BSE}$. If such a crust-contaminated
461 mantle experiences a new partial melting process, it is possible to obtain melts with a wide range of
462 isotopic compositions, with values lower to much higher than the BSE estimate.

463 In conclusion, the $^{87}\text{Sr}/^{86}\text{Sr}$ ratios of igneous rocks can be used to constrain the depleted (low
464 $^{87}\text{Sr}/^{86}\text{Sr}$, indicating long-time evolution of a low Rb/Sr system, indicating old melt extraction, with
465 Rb more incompatible than Sr) or the enriched (high $^{87}\text{Sr}/^{86}\text{Sr}$, indicating, high Rb/Sr) character of
466 their sources. This can be done quantitatively only if the age of the melt extraction events, their
467 number, the amount of the melt extracted (the Rb/Sr of the melt varying as function of the degree of
468 melting), the age of the recycling process during subduction, the isotopic and elemental
469 composition of the original crustal material entering the trench, the metamorphic reactions in the
470 subducting slab (able to fractionate Rb from Sr) and the style of interaction between fluids/melts
471 released from the slab with the supra-subduction mantle wedge are precisely known. This is never
472 the case. These factors can only be estimated, guessed or assumed and as a consequence the results
473 of a geochemical modelling are only qualitative or semi-quantitative at best.

474 Partial melting decreases the $^{87}\text{Rb}/^{86}\text{Sr}$ ratios of the mantle residuum, ultimately resulting in
475 $^{87}\text{Sr}/^{86}\text{Sr}$ ratios $<\text{BSE}$. Recycling of upper crustal lithologies increases $^{87}\text{Rb}/^{86}\text{Sr}$ and the $^{87}\text{Sr}/^{86}\text{Sr}$
476 ratio of the supra-subduction mantle wedge, forcing it to higher $^{87}\text{Sr}/^{86}\text{Sr}$ ratios and towards values
477 $>\text{BSE}$. What is clear is that the $^{87}\text{Sr}/^{86}\text{Sr}$ isotopic composition of an igneous rock $<\text{BSE}$ clearly
478 indicates derivation from a mantle source that has experienced partial melt extraction in its past, and
479 $^{87}\text{Sr}/^{86}\text{Sr}$ ratios $>\text{BSE}$ indicate derivation from a mantle that is not primitive.

480 Despite these simple considerations, $^{87}\text{Sr}/^{86}\text{Sr}$ ratios in basalts as low as 0.7025 are considered to
481 reflect derivation from enriched end-members classically identified with deep mantle upwelling in
482 the form of mantle plumes (e.g., Merle et al., 2009). Ironically, such low $^{87}\text{Sr}/^{86}\text{Sr}$ values (coupled
483 with high $^{143}\text{Nd}/^{144}\text{Nd}$ ratios, see below) were originally regarded as evidence of derivation from a
484 depleted MORB-like source (e.g., Gast, 1968).

485

486 **The Sm-Nd isotope system.** Samarium and Neodymium belong to the Rare Earth Element (REE)
487 group, a suite of 14 incompatible elements all with the same charge with atomic number (Z)
488 increasing from La (Z = 57) to Lu (Z = 71). The ionic radius of the REE decreases slightly from La
489 (1.17 Å) to Lu (1.00 Å). The same +3 valence of Nd (Z = 60) and Sm (Z = 62), but the slightly
490 lower ionic radius of the latter (1.12 Å vs. 1.10 Å for Nd and Sm, respectively), renders Nd slightly
491 more incompatible than Sm during mantle partial melting and basaltic melt crystallization (Fig. 3).
492 Samarium is present in seven different isotopes with masses 144 (3.1%), 147 (15%), 148 (11.2%),
493 149 (13.8%), 150 (7.4%), 152 (26.7%) and 154 (22.7%), of which only ^{147}Sm and ^{148}Sm are
494 radioactive.

495 The half-life of ^{148}Sm is very long (7×10^{15} yr) and consequentially it can be considered to be a
496 stable element on the timescale of the Earth. On the other hand, the half-life of ^{147}Sm is shorter
497 (1.06×10^{11} yr) and its decay chain is relevant to geology. ^{147}Sm is transformed by α -decay into
498 ^{143}Nd and the ^{147}Sm - ^{143}Nd system works in the same way of the ^{87}Rb - ^{87}Sr system discussed above
499 (Table 1). Given the higher half-life of ^{147}Sm (106 Gyr) compared to that of ^{87}Rb (48 Gyr), less
500 ^{143}Nd than ^{87}Sr has been produced during Earth's lifetime. In absolute terms, however, the number
501 of radiogenic ^{143}Nd atoms (15% of all the Nd isotopes) produced in 4.56 Gyr is higher than the
502 number of radiogenic ^{87}Sr atoms because of the higher amount of ^{147}Sm compared with ^{87}Rb (7% of
503 all the Rb isotopes). The only substantial difference with the Rb-Sr system is that the radioactive
504 (parent) isotope (^{147}Sm) is less incompatible than the radiogenic (daughter) isotope ^{143}Nd . The
505 definition "less incompatible" is here preferred to "more compatible" to highlight the general
506 incompatible character of both Sm and Nd during peridotite partial melting.

507 Also in this case the radiogenic ^{143}Nd isotope is measured against a stable Nd isotope (^{144}Nd)
508 according to the classical relation $^{143}\text{Nd}/^{144}\text{Nd}$. The Earth's primordial $^{143}\text{Nd}/^{144}\text{Nd}$ isotopic ratio is
509 assumed to be the same as chondritic meteorites and is constrained to 0.512638 (defined as ChUR =

510 Chondritic Uniform Reservoir), while the $^{143}\text{Nd}/^{144}\text{Nd}$ at the time of formation of the solar system
511 was 0.50669. In other words, $^{143}\text{Nd}/^{144}\text{Nd}$ during the last 4.56 Gyr has increased by 0.00595.

512 Several attempts have been made to modify the accepted concept of chondritic Earth to solve the
513 problem raised by another Nd isotope (^{142}Nd), suggesting for the whole Earth a $^{143}\text{Nd}/^{144}\text{Nd}$ isotopic
514 ratio more radiogenic than ChUR (0.5130; Caro and Bourdon, 2010; Jackson and Jellinek, 2013). It
515 is worth noting, however, that any modification of the accepted chondritic Earth assumption raises a
516 large number of additional problems (e.g., for a super-chondritic $^{143}\text{Nd}/^{144}\text{Nd}$ value for the Earth,
517 the depleted major- and trace-element content of MORB would be at odds with their “new”
518 primitive Nd isotopic composition). As a consequence, we continue using the classically accepted
519 chondritic (ChUR) value.

520 Nd is slightly more incompatible than Sm during partial melting, so a restitic mantle is
521 characterized by lower Nd/Sm (and hence higher $^{147}\text{Sm}/^{144}\text{Nd}$) than the pre-melting composition
522 and the basaltic melt. A rock with high $^{147}\text{Sm}/^{144}\text{Nd}$ will evolve, with ageing, to high $^{143}\text{Nd}/^{144}\text{Nd}$
523 isotopic ratios (Fig. 3). Following the rationale described for the Rb/Sr isotopic system, an anciently
524 depleted mantle source will be characterized by $^{143}\text{Nd}/^{144}\text{Nd}$ higher than ChUR and much higher
525 than solidified partial melt (characterized by lower Sm/Nd, i.e., lower ^{147}Sm , and consequentially
526 lower ^{143}Nd produced for a given amount of stable ^{144}Nd). Also in this case, igneous rocks
527 interpreted as the products of mantle plumes, tapping primitive mantle sources should be
528 characterized by $^{143}\text{Nd}/^{144}\text{Nd}$ ratios very close to ChUR. However, they are nearly constantly shifted
529 towards isotopically depleted (i.e., $^{143}\text{Nd}/^{144}\text{Nd} > \text{ChUR}$) compositions ruling out the existence of
530 such primitive mantle compositions.

531 The Sr-Nd isotopic pair is at the base of isotope geochemistry applied to igneous petrology. All
532 basaltic compositions, erupted in oceanic or continental intra-plate settings plot along a trend,
533 defined originally as the mantle array (e.g., Sun, 1980; Figs. 4, 5a). This connects the isotopically
534 depleted field (characterized by $^{87}\text{Sr}/^{86}\text{Sr} < \text{BSE}$ and $^{143}\text{Nd}/^{144}\text{Nd} > \text{ChUR}$) with the isotopically
535 enriched field ($^{87}\text{Sr}/^{86}\text{Sr} > \text{BSE}$ and $^{143}\text{Nd}/^{144}\text{Nd} < \text{ChUR}$), passing through BSE-ChUR values (Fig.
536 4). MORBs plot entirely in the depleted field, HiMu-OIB plot nearly entirely in the depleted
537 isotopic field, while EMI- and EMII-OIB extend to the enriched field (Fig. 5a).

538 In Fig. 5a a recent compilation of oceanic basalt isotopic data (Stracke, 2012) is plotted together
539 with the four basic colors of the mantle isotopic printer. The DMM-HiMu-EMI-EMII irregular
540 quadrilateral envelops >99% of oceanic basalts. As a consequence, their Sr-Nd isotopic

541 composition can be simply explained in terms of the relative contribution of these four extreme
542 values. This is the basis of isotope geochemistry applied to the petrogenesis of oceanic (and also
543 continental, Fig. 5b) basalts. Up to this point there is no fundamental disagreement between the
544 geochemical and petrological communities except for the precise position of the four end-members
545 in Sr-Nd-Pb isotopic space. Problems emerge when trying to translate into geological terms these
546 four end-members, assigning thermal, rheological, physical, depth and mineralogical meaning to
547 these “colors”.

548

549 **The U-Th-Pb isotope system.** The Uranium-Thorium-Lead system is more complex than the
550 Rb/Sr and Sm/Nd systems. Here there are three radiogenic isotopes (^{235}U , ^{238}U and ^{232}Th) that
551 decay into three different radiogenic Pb isotopes (^{206}Pb , ^{207}Pb , ^{208}Pb , respectively), with different
552 half-lives and energy emissions. Uranium is present as two radioactive isotopes with masses 235
553 (0.72%) and 238 (99.28%). Thorium is present only as ^{232}Th , while Pb is present as four stable
554 isotopes with masses 204 (1.4%), 206 (24.1%), 207 (22.1%) and 208 (52.4%).

555 As discussed previously, the ^{206}Pb , ^{207}Pb and ^{208}Pb abundances slowly but continuously increase
556 due to the decay of ^{235}U (half-life = 0.7 Gyr), ^{238}U (4.5 Gyr) and ^{232}Th (14.0 Gyr). In this case the
557 three radiogenic Pb isotopes are normalized to one of the stable Pb isotopes, ^{204}Pb . As a
558 consequence, the U-Th-Pb isotopic system is conventionally reported as three separate isotopic
559 ratios: $^{206}\text{Pb}/^{204}\text{Pb}$, $^{207}\text{Pb}/^{204}\text{Pb}$ and $^{208}\text{Pb}/^{204}\text{Pb}$. The $^{238}\text{U}/^{204}\text{Pb}$ isotopic ratio is defined as μ (mu),
560 while the $^{232}\text{Th}/^{238}\text{U}$ is defined as κ (kappa). Strictly speaking, the Greek letter μ should be spelled
561 as “mi”, not “mu”. This means that the classical HiMu mantle end-member should be defined as
562 “HiMi”. The Earth’s $^{238}\text{U}/^{235}\text{U}$ ratio is 137.88.

563 Given that the ^{235}U half-life is much shorter than that of ^{238}U , $^{207}\text{Pb}/^{204}\text{Pb}$ increases more rapidly
564 than $^{206}\text{Pb}/^{204}\text{Pb}$. As a consequence, in a $^{207}\text{Pb}/^{204}\text{Pb}$ vs. $^{206}\text{Pb}/^{204}\text{Pb}$ plot the Pb isotopic evolution
565 (i.e., the Pb isotopic ratios of a rock with increasing age) follows a convex-upward curve (Fig. 6a).

566 Let us assume that the early Earth, with initial solar $^{206}\text{Pb}/^{204}\text{Pb}$ and $^{207}\text{Pb}/^{204}\text{Pb}$ ratios X0 and Y0,
567 respectively (Fig. 6a), evolved as a single system (i.e., without any differentiation process such as
568 partial melting) for a period t_1 with a $^{238}\text{U}/^{204}\text{Pb}$ ratio = μ_1 (Fig. 6a). After a time t_1 the new Pb
569 isotopic composition of the Earth would be X1,1 and Y1,1 (Fig. 6a). If the Earth, during this period
570 had a different μ value (e.g., $\mu_2 > \mu_1$), but the same initial Pb isotopic composition, after the same
571 time t_1 it would have had different (higher) Pb isotopic ratios (X1,2 and Y1,2; Fig. 6a). The dashed

572 line t_0 - t_1 , obtained by connecting the isotopic composition of different reservoirs with the same
573 initial Pb isotopic composition, but with different μ , represents the *isochron* after time t_1 .

574 What happens if the same uniform reservoirs (assumed to evolve with $^{238}\text{U}/^{204}\text{Pb}$ ratios μ_1 or μ_2
575 but the same initial isotopic ratios) allow Pb isotopic ingrowth for an additional time t_2 ? After this
576 additional time, both the hypothetical reservoirs (with μ_1 or μ_2) will be characterized by higher
577 $^{206}\text{Pb}/^{204}\text{Pb}$ and $^{207}\text{Pb}/^{204}\text{Pb}$ ratios. Obviously, sources with μ_2 will be characterized by more ^{206}Pb
578 and ^{207}Pb , having higher U/Pb. At a time t_2 the Pb isotopic composition of a system with μ_1 will be
579 X2,1 and Y2,1, while a system with μ_2 will be X2,2 and Y2,2 (Fig. 6a). The dashed line connecting
580 t_0 and t_2 represents the *isochron* at t_2 .

581 Present day Earth ($t_3 = 4.56$ Gyr), with hypothetical μ_1 or μ_2 , should have $^{206}\text{Pb}/^{204}\text{Pb}$ at X3,1 and
582 X3,2, and $^{207}\text{Pb}/^{204}\text{Pb}$ ratios at Y3,1 and Y3,2, respectively (Fig. 6a). Whatever the μ of the Earth,
583 the *total* Pb isotopic composition of our planet *must* plot on the isochron t_3 . The isochron at 4.56
584 Gyr is defined as the *meteoritic isochron* or *Geochron*. The entire solar system (as determined by
585 the composition of meteorites) plots on the 4.56 Gyr Geochron, with $^{206}\text{Pb}/^{204}\text{Pb}$ ratios ranging from
586 ~ 10 to ~ 50 and $^{207}\text{Pb}/^{204}\text{Pb}$ ratios ranging from ~ 9 to ~ 37 . This does not mean that *all* the Earth's
587 rocks must plot on the Geochron.

588 In principle rocks can plot on the left or on the right of the Geochron. The various shells of the
589 Earth (crust, mantle, core) have a common origin (i.e., the same primordial solar Pb isotopic
590 composition; X0 and Y0 in Fig. 6a), but have accreted or consumed at different times and evolved
591 with different μ values. In particular, these reservoirs evolved with different $^{207}\text{Pb}/^{204}\text{Pb}$, $^{206}\text{Pb}/^{204}\text{Pb}$
592 and $^{208}\text{Pb}/^{204}\text{Pb}$ ratios.

593 Each partial melting stage (i.e., to produce new crustal material) produces at least two different
594 new sources characterized by different U/Pb (and μ) that will evolve with fast (high μ) or slow (low
595 μ) producing variable ^{207}Pb and ^{206}Pb isotopic growth. Let us assume that a uniform system evolved
596 with primordial solar system Pb isotopic ratios for a time t_2 and a $^{238}\text{U}/^{204}\text{Pb}$ ratio = μ_1 . Its isotopic
597 composition is indicated by the white star in Fig. 6b. If a partial melting event occurs, this originally
598 uniform system is split into two reservoirs, one evolving with low $^{238}\text{U}/^{204}\text{Pb}$ (the restitic mantle)
599 and the other with high $^{238}\text{U}/^{204}\text{Pb}$ (the partial melt). The elemental fractionation between U and Pb
600 happens because the two elements have slightly different compatibility in mantle minerals and,
601 consequentially, they are fractionated by partial melting and fractional crystallization processes.

602 Assuming that $t_2 = 2$ Gyr, these two complementary reservoirs (the mantle residuum and the
603 solidified partial melt) will evolve up to the present day with different μ , but the same initial Pb
604 isotopic composition. After 2.56 Gyr, the two reservoirs will have different isotopic compositions,
605 represented by the star labelled R1 (Residuum) and M1 (Melt). The total Pb isotopic composition of
606 the two systems must plot on the intersection between the Geochron and the R1-M1 segment.
607 Similarly, if the original isotopic system evolved with higher $^{238}\text{U}/^{204}\text{Pb}$ (μ_2), a partial melt
608 extraction at $t_2 = 2$ Gyr will produce, at $t_3 = 4.56$ Gyr, two systems R2 and M2 (Fig. 6b). Whatever
609 the original μ and the μ produced during partial melt formation, the total composition of the system
610 must plot somewhere along the Geochron.

611 It is important to understand that the whole Earth system, not the single solid reservoirs, must plot
612 along the Geochron. During the Earth's chemical stratification, the upper crust evolved with higher
613 U/Pb (given that U is slightly more incompatible than Pb during partial melting processes) and the
614 residual mantle evolved towards lower U/Pb. This, coupled with the different initial Pb isotopic
615 compositions of these two most extreme reservoirs, means that upper crustal rocks, having higher
616 U/Pb are also characterized by higher μ and, consequentially, should plot somewhere to the right of
617 the Geochron.

618 On the other hand, residual mantle rocks, characterized by lower μ , should have retarded ^{207}Pb and
619 ^{206}Pb isotopic growth, and consequentially they should plot to the left of the Geochron. What is
620 anomalous is that both upper crustal rocks (various estimates grouped in the small orange field in
621 Fig. 6a) and depleted mantle rocks (or partial melts, i.e., MORB; part of the yellow field in Fig. 6a)
622 all plot to the right of the Geochron. Also >99.9% of OIB plot on or to the right of the Geochron
623 (OIB and MORB grouped with the same yellow field in Fig. 6a). This is called the first Pb paradox
624 (Allègre, 1969).

625 If both partial melts and residual mantle compositions all plot to the right of the Geochron, some
626 hidden or poorly represented reservoir must exist somewhere. This reservoir must be placed well to
627 the left of the Geochron, so that the whole Earth Pb isotopic composition plots somewhere along
628 this line. The only terrestrial reservoir characterized by compositions plotting to the left of the
629 Geochron (and characterized by low to extremely low $^{206}\text{Pb}/^{204}\text{Pb}$, down to ~ 10 and $\mu \sim 0$) is the
630 ancient lower continental crust.

631 In Fig. 6a both the fields of ancient lower crustal xenoliths (sky blue field) and the model old
632 continental crust (star; Lustrino, 2005; Bolhar et al., 2007) are shown. The metamorphic reactions

633 occurring during basalt to granulite/eclogite facies are indeed characterized by U/Pb fractionation,
634 with U leaving the system more easily than Pb. The consequence is that a metamorphosed (eclogitic
635 s.l.) lower crust is characterized by very low μ and consequentially its $^{206}\text{Pb}/^{204}\text{Pb}$ (but also
636 $^{207}\text{Pb}/^{204}\text{Pb}$) remains virtually frozen and does not increase with time, as there is little if any ^{238}U
637 (and ^{235}U). If such an eclogitization process is old, the Pb isotopic ratios are stopped at their infant
638 stage, close to values more similar to primordial solar system values ($^{206}\text{Pb}/^{204}\text{Pb} = 10.29$;
639 $^{207}\text{Pb}/^{204}\text{Pb} = 9.31$) than the typical igneous rock range ($^{206}\text{Pb}/^{204}\text{Pb} \sim 17-21$; $^{207}\text{Pb}/^{204}\text{Pb} = \sim 15.2-$
640 15.8 ; $\mu = 4-16$).

641 Foundering of this dense lithology (which is much denser than the shallow lithospheric mantle) in
642 the form of a mafic keel in overthickened collision zones can explain the extreme rarity of these
643 compositions on the Earth's surface. This dense eclogite may be now stored in the TZ, as originally
644 proposed by Anderson (1989).

645 The lead isotope system is particularly important in basalt petrogenesis especially because it is
646 considered to be one of the milestones of geochemical mantle plume modelling, suggesting lower
647 mantle derivation for OIB. Ironically, it was Pb isotopes that led Tatsumoto (1978) to conclude that
648 OIB were from the shallow mantle and MORB from the deeper mantle, thus agreeing with the
649 classical physics-based models (e.g., Birch, 1952).

650 Two of the four "colors" of the Earth's mantle (i.e., the mantle end-members manifested in
651 oceanic basalts away from subduction zones) are essentially identified on Pb isotopic grounds. One
652 of these colors is represented by the EMI end-member (e.g., Lustrino and Dallai, 2003), whose type
653 localities are identified in the Pitcairn islands and seamounts in French Polynesia (e.g., Woodhead
654 et al., 1993), the east-central Atlantic Ocean (Walvis Ridge; Salters and Sachi-Kocher, 2010), some
655 SW Indian ridge sectors, the Aphanasy-Nikitin seamount chain (Mahoney et al., 1996; Borisova et
656 al., 2001) and the Ko'olau-stage lavas of Oahu island (Hawaii; Tanaka et al., 2002; Huang and
657 Frey, 2005). This hypothetical mantle end-member is characterized by its peculiar low $^{206}\text{Pb}/^{204}\text{Pb}$
658 (down to ~ 16.7 ; Fig. 7), associated with non-unique mildly radiogenic $^{87}\text{Sr}/^{86}\text{Sr}$ and strongly
659 unradiogenic $^{143}\text{Nd}/^{144}\text{Nd}$ (Fig. 5).

660 The other mantle color/end-member defined on the grounds of Pb isotopes is HiMu, represented
661 by a very rare group of rocks cropping out in French Polynesia (Rurutu, Tubuai and Mangaia
662 islands; Chauvel et al., 1995; Stracke et al., 2005; Hanyu et al., 2013) and, with less extreme
663 compositions, on the island of St. Helena (Kawabata et al., 2011; Hanyu et al., 2014). The HiMu

664 end-member is characterized by the most radiogenic Pb isotopic compositions recorded in oceanic
665 basalts (Fig. 7a). The other two colors of the mantle isotopic printer are EMII and DMM.

666 The EMII mantle end-member is characterized by $^{206}\text{Pb}/^{204}\text{Pb}$ intermediate between EMI and
667 HiMu (~ 19) and relatively high $^{207}\text{Pb}/^{204}\text{Pb}$ for a given $^{206}\text{Pb}/^{204}\text{Pb}$ (Fig. 7a). The relative $^{207}\text{Pb}/^{204}\text{Pb}$
668 enrichment of EMII lavas can be mathematically shown as a positive $\Delta 7/4\text{Pb}$ value, a parameter
669 proposed by Hart (1984) to emphasize the vertical shift of southern hemisphere oceanic basalts
670 compared with northern ones (defining the so-called NHRL, Northern Hemisphere Reference Line)
671 in $^{207}\text{Pb}/^{204}\text{Pb}$ vs. $^{206}\text{Pb}/^{204}\text{Pb}$ plots (Fig. 7a). The vertical shift from the NHRL (that can be
672 identified also for $^{208}\text{Pb}/^{204}\text{Pb}$; $\Delta 8/4\text{Pb}$) is also defined as the DupAl anomaly (after the two
673 researchers who first described it; Dupré and Allegre, 1983).

674 The last color of the mantle isotopic printer is DMM (Fig. 7a). This “color” is by far the most
675 common and nearly always present in portraits of oceanic and continental intra-plate basalts. It is
676 also a constant feature of partial melts generated in supra-subduction mantle wedges. Despite the
677 fact that DMM is necessary in almost every recipe to model oceanic basalts, the Pb isotopic
678 composition of DMM is not well constrained. Indeed, there have been several attempts to estimate
679 the $^{206}\text{Pb}/^{204}\text{Pb}$, $^{207}\text{Pb}/^{204}\text{Pb}$ and $^{208}\text{Pb}/^{204}\text{Pb}$ of this end-member, with estimates ranging from ~ 16.8
680 to ~ 18.4 ($^{206}\text{Pb}/^{204}\text{Pb}$), from ~ 15.3 to ~ 15.4 ($^{207}\text{Pb}/^{204}\text{Pb}$) and from ~ 36.5 to ~ 38 ($^{208}\text{Pb}/^{204}\text{Pb}$). The
681 quadrilateral with the four mantle end-members at the apexes also envelopes continental rocks, as
682 shown in Fig. 7b. Surprisingly, from a mantle plume point of view, DMM is not a focal point on
683 isotope plots, i.e. trends do not converge toward DMM compositions. They converge toward FOZO
684 (Focal Zone) or C (Common component; Stracke et al., 2005; Jackson et al., 2014).

685 The Sr-Nd isotopic resemblance between DMM and HiMu (plotting in the same depleted field)
686 disappears when observing these two end-members from different perspectives (i.e., Pb isotopes).
687 Fig. 7 clearly indicates their different origins. The position of the DMM reservoir is compatible
688 with a U-depleted composition, while the extremely radiogenic $^{206}\text{Pb}/^{204}\text{Pb}$ (but also of the other Pb
689 isotopic pairs) of the HiMu end-member requires high U/Pb and Th/Pb in their genesis. This is
690 classically attributed to recycling of Pb-poor lithologies in the deep mantle, in regions not involved
691 in strong convective systems (e.g., Chauvel et al., 1992, 1995). These Pb-poor lithologies probably
692 are hydrothermally-altered oceanic crust where Pb was first concentrated in sulphides which were
693 then removed when the slab entered the trench. The oceanic crust residuum would be, as a
694 consequence, characterized by high U/Pb, not because of elevated U content, but rather because of

695 low Pb. Storage of such high U/Pb lithologies and insulation for long periods would allow
696 radiogenic growth of ^{206}Pb and ^{207}Pb , which are the most striking characteristics of the HiMu end-
697 member (Fig. 7). In other words, the Pb isotopic composition of the HiMu end-member (classically
698 identified as the strongest geochemical evidence for a mantle plume) requires long periods of
699 insulation of high U/Pb lithologies, not thermal anomalies or deep sources. With the present state of
700 knowledge, it is not possible to say that a given Pb isotopic composition is proof for the existence of
701 a mantle plume as often used as an *a priori* conjecture.

702

703 **The U-Th-He isotope system.** Helium is the lightest noble gas, present in two isotopes, ^3He and
704 ^4He , whose ratios in igneous rocks are classically used to constrain mantle structure and infer its
705 evolution (e.g., Ballentine, 2012). ^3He is the primordial isotope trapped inside the Earth during its
706 accretion, and is continuously escaping from the Earth's surface when mantle melts degas at
707 shallow depths. During the decay into stable Pb isotopes, ^{235}U , ^{238}U and ^{232}Th produce ^4He isotopes
708 as α -particles. Helium isotopes are classically reported as $^3\text{He}/^4\text{He}$ ratios (R) over atmospheric
709 $^3\text{He}/^4\text{He}$ ($R_a = 1.38 \times 10^{-6} \text{ cm}^3/\text{g}$). This reverses the usual geochemical convention of the unstable
710 isotope (e.g., ^{87}Sr or ^{143}Nd) normalized to the stable isotope (e.g., ^{86}Sr or ^{144}Nd). In the case of
711 Helium the stable isotope (^3He) is normalized to the unstable one (^4He). This convention is carried
712 over into the interpretation of $^3\text{He}/^4\text{He}$ ratios where variation in ^4He is usually not considered and
713 high $^3\text{He}/^4\text{He}$ is typically attributed to high ^3He derived from a deep-sourced, undegassed mantle
714 region (e.g., Davies, 2011). Despite increasing criticism in using He isotope systematic to infer the
715 existence of primordial deep-mantle reservoirs for "plume magmas" (White, 2010), high $^3\text{He}/^4\text{He}$
716 ratios in basaltic melts continue to be considered the strongest isotopic signal of a deep mantle
717 provenance of their sources (Jackson et al., 2014).

718 MORB are characterized by $^3\text{He}/^4\text{He}$ ratios (R/Ra) ranging from ~ 1 to ~ 22 , but with nearly all the
719 samples concentrated in the narrow interval 8 ± 1 R/Ra (e.g., Meibom et al., 2003; Graham et al.,
720 2014). In contrast to MORB, magmas emplaced in oceanic and continental intra-plate settings are
721 characterized by variable $^3\text{He}/^4\text{He}$ ratios, with R/Ra ranging from ~ 5 to ~ 50 and a poor correlation
722 with other isotope systematics (e.g., Rb-Sr, Sm-Nd, U-Th-Pb) and incompatible trace element ratios
723 (e.g., Peters and Day, 2014). This can be understood in part from the central limit theorem (high
724 degree melts and large volume samples average over large volumes and have smaller variances) and

725 from the fact that helium isotope ratios are partly controlled by degassing as well as by melting
726 (Meibom et al., 2003).

727 Earth materials are characterized by $^3\text{He}/^4\text{He}$ ratios much lower (<50 R/Ra) than the cosmic solar
728 wind (~ 310 R/Ra) because of the continued ^3He loss and the continued ^4He production by
729 radioactive decay. Plate tectonics moves primordial ^3He from the Earth's interior to the surface via
730 partial melting and degassing, while subduction recycles back to the mantle ^4He in the form of U-
731 Th-rich crustal lithologies. The result is that the $^3\text{He}/^4\text{He}$ ratio of the Earth has been continuously
732 decreasing since the Earth's accretion (Fig. 8a). The two exceptions are in sediments that are rich in
733 cosmic spherules (solar ^3He -rich) and in lithium-rich rocks (e.g., Smith, in press).

734 Despite the common view (e.g., Gonnermann and Mukhopadhyay, 2009; Davies, 2011;
735 Ballentine, 2012), high $^3\text{He}/^4\text{He}$ ratios indicate high time-integrated $^3\text{He}/(\text{Th}+\text{U})$ ratios, not
736 automatically high absolute ^3He content. Similarly, low $^3\text{He}/^4\text{He}$ ratios are not proof of absolute low
737 ^3He content. Relatively low $^3\text{He}/^4\text{He}$ ratios in MORB have been related to relatively U+Th-rich
738 concentrations associated with variable He loss through magma degassing in the upper mantle (i.e.,
739 ^4He -rich rather than ^3He -poor; Meibom et al., 2003) and the presence of He-rich bubbles trapped in
740 cavities and nucleating on the surface of early-forming olivine crystals (Natland, 2003). Similarly,
741 high $^3\text{He}/^4\text{He}$ ratios can result from ancient Th+U-poor sources, resulting in low ^4He production
742 with time, while low $^3\text{He}/^4\text{He}$ ratios can result from sources with ancient Th- and U-rich lithologies.

743 Despite these obvious considerations, the scientific literature is full of claims such as: “*Helium is a*
744 *powerful tracer of primitive material in Earth's mantle. Extremely high $^3\text{He}/^4\text{He}$ ratios in some*
745 *ocean-island basalts suggest the presence of relatively undegassed and undifferentiated material*
746 *preserved in Earth's mantle*” (Jackson et al., 2010); “*Hot-spot magmas often have elevated values*
747 *in the ratio of primordial helium to radiogenic helium ($^3\text{He}/^4\text{He}$), which indicates their source is in*
748 *a part of the mantle that has not lost its dissolved gases to the atmosphere.*” (Humphreys and
749 Schmandt, 2011); “*The existence of different $^4\text{He}/^3\text{He}$ ratios underpins the idea that there are at*
750 *least two geochemical reservoirs in the mantle: a deep reservoir rich in gases and volatile*
751 *compounds feeds material into an upper reservoir, which is the convecting part of the mantle that*
752 *supplies magma to mid-ocean ridges*” (Ballentine, 2012); “[...] *the less-degassed mantle source*
753 *traced by high $^3\text{He}/^4\text{He}$. [...] He isotopes provide direct evidence for the preservation of relatively*
754 *undegassed, primordial reservoirs in the present-day mantle.*” (Peters and Day, 2014).

755 More evolved views interpret both high $^3\text{He}/^4\text{He}$ and low $^3\text{He}/^4\text{He}$ ratios as being derived from
756 deep mantle plumes, the first representing the true plume matrix and the second representing the
757 “*subducted materials – oceanic crust, mantle lithosphere and sediments – which may also reside in*
758 *slab graveyards at the bottom of the mantle where plumes originate*” (Jackson et al., 2014). In other
759 words, whatever the $^3\text{He}/^4\text{He}$ ratios are measured in mantle melts (as low as 5 or as high as 50
760 R/Ra) they are considered to represent a proof for a deep mantle provenance.

761 Focusing on the elemental He content in basalt phenocrysts (mostly clinopyroxene and olivine) it
762 emerges that OIB have a much lower ^3He (typically around 10^{-14} to 10^{-11} cm^3/g) compared with
763 MORB (typically around 10^{-11} to 10^{-9} cm^3/g ; Ozima and Igarashi, 2000; Hanyu et al., 2005; Mourao
764 et al., 2012; Hanyu, 2014). Despite this, it is commonly believed that “*The MORB source contains*
765 *less ^3He because it was degassed in Early Earth history*” (Moreira et al., 2012) and that high
766 $^3\text{He}/^4\text{He}$ ratios reflect lower mantle chemical signatures in continental settings (e.g., the Columbia
767 River Basalts; Camp, 2013). There is no reason to believe that MORB sources are depleted in ^3He
768 compared with postulated primitive and undegassed-plume-related OIB sources (Anderson, 1998,
769 2007; Ozima and Igarashi, 2000). On this basis, statements such as “*Large, long-lived, ^3He -rich*
770 *plumes, and especially those that have generated enormous volumes of oceanic or continental flood*
771 *basalts, are more likely to have come from the base of the lower mantle*” (Hofmann, 1997) need
772 rethinking. The actual very low ^3He content of postulated “plume magmas” (i.e., up to five orders of
773 magnitude less than what is recorded in MORB) has been related to the subaerial activity of OIB, a
774 characteristic that would favour preferential noble gas escape from magma compared with MORB,
775 erupted at high water depths (and therefore high pressures, preventing degassing). This solution is
776 not viable because OIB should also have much higher $^3\text{He}/^{36}\text{Ar}$ than MORB (the higher the mass of
777 the noble gas, the less its melt compatibility; e.g., Carrol and Draper, 1994), while actually MORB
778 are characterized by higher $^3\text{He}/^{36}\text{Ar}$ ratios, with no correlation between ^3He and ^{36}Ar (Ozima and
779 Igarashi, 2000). The fact that the highest $^3\text{He}/^4\text{He}$ ratios (~ 50 R/Ra) are recorded in Mg-rich, alkali-
780 poor picritic magmas (Baffin Island; NE Canada characterized by very low $^{87}\text{Sr}/^{86}\text{Sr}$ (~ 0.7031) and
781 very high $^{143}\text{Nd}/^{144}\text{Nd}$ (~ 0.5130 ; Stuart et al., 2003), indicate an important role of depleted mantle
782 sources in their petrogenesis. The depleted (i.e., not primitive nor undegassed) source is also
783 testified by low LREE/MREE ratios (LREE = Light Rare Earth Elements; MREE = Medium REE,
784 e.g., La/Sm < 0.6).

785 The apparent conundrum of invoking undegassed sources in the petrogenesis of alkali-poor, Sr-
786 unradiogenic and Nd-radiogenic basaltic melts is solved by proposing mixing between depleted
787 upper mantle (responsible for all the geochemical characteristics of the Baffin Island picrites, also
788 apparent in the mineral chemistry) and a gas-rich (^3He -rich) component (Stuart et al., 2003). The
789 linear correlation between He-Sr and He-Nd isotopes should indicate a perfect He elemental
790 distribution in the two mixing end-members, which is difficult to understand invoking DMM and
791 primitive mantle regions (as a “plume head dispersed in the upper mantle”) to represent these two
792 end-members. The Baffin Island picrites are important because they are considered to be the first
793 product of the proto-Icelandic mantle plume (e.g., Graham et al., 1998; Stuart et al., 2003; Jackson
794 et al., 2010).

795 The mantle plume hypothesis has received support from the conclusions of many noble gas
796 geochemists who have proposed a direct link between high $^3\text{He}/^4\text{He}$ ratios with high absolute ^3He
797 and, as a consequence, a primitive and relatively undegassed source (White, 2010; Jackson et al.,
798 2010; Ballentine, 2012; Class and Goldstein, 2005). Alternatively, the origin of a ^3He -rich lower
799 mantle is considered not a primary feature, but, rather, related to accumulation of recycled oceanic
800 basalts and hybrid pyroxenites rich in ^3He (Davies, 2011). The supposed high abundance in ^3He of
801 oceanic crust recycled down to D" is based on the assumption that He is strongly partitioned to
802 melts during shallow mantle melting beneath oceanic ridges. While this is certainly true, this model
803 cannot explain: 1) the differences between MORB and “lower mantle-derived”-OIB; 2) the lower
804 absolute abundance of ^3He in OIB compared to MORB and 3) the radiogenic ingrowth of ^4He due
805 to the decay of U and Th isotopes that would decrease the $^3\text{He}/^4\text{He}$ in the mantle plume-related OIB.

806 In some cases $^3\text{He}/^4\text{He}$ ratios in the range 6.5-10.6 R/Ra and ^3He contents as low as 10^{-3} cm³/g
807 have been considered, together with other noble gas arguments, as sufficient proof for the presence
808 of deep-rooted mantle plumes below Hawaii and the Louisville seamount chain (Hanyu, 2014).
809 According to this view the U-Th-He isotopic system is related to the different compatibility of
810 U+Th with respect to He, in rocks and magmas (degassing fractionation between U, Th, He and
811 other noble gases being ignored). The two different approaches are reviewed by Parman et al (2005)
812 (Fig. 8a,b). The continuous thick line evolving from ~130 R/Ra (at ~4.5 Ga) to ~50 R/Ra (Present)
813 indicates the evolution of a Th+U-bearing undegassed mantle. Partial melts of this undegassed
814 mantle should be characterized by relatively high R/Ra values, indicated with black dot 1
815 (representing the highest $^3\text{He}/^4\text{He}$ measured in igneous rocks; Stuart et al., 2003). A hypothetical

816 partial melting event at 2 Ga would produce a liquid and a mantle residuum. Both He and the U+Th
817 pair are strongly incompatible during mantle partial melting, but the standard model assumes
818 stronger incompatibility of He with respect to both U and Th. This means that partial melts have
819 higher He/(U+Th) than either the undegassed mantle or the mantle residuum. Such a partial melt
820 would be subject to degassing at shallow depths, allowing preferential escape of He from the melt
821 and resulting in a ~1000-fold reduction of the original He/(Th+U) ratio (Parman et al., 2005). The
822 isotopic evolution of this degassed melt is indicated with the dashed line in Fig. 8a. The mantle
823 residuum would be characterized by lower He/(Th+U) ratios than undegassed mantle and partial
824 melts. The evolution of this depleted (degassed) reservoir would evolve towards relatively low
825 $^3\text{He}/^4\text{He}$ (R/Ra ~8) like that recorded in present-day MORB (Fig. 8a). In the alternative model U
826 and Th are up to two orders of magnitude more incompatible than He during partial melting
827 ($D^{\text{Th,U}} < D^{\text{He}}$; Parman et al., 2005). The partial melt would evolve more or less in the same way as the
828 standard model, with shallow-depth magma degassing the controlling mechanism to produce He-
829 poor, He/(Th+U)-poor melts evolving with age towards very low $^3\text{He}/^4\text{He}$ ratios. The difference
830 from the standard model rests in the fact that in this case the degassed reservoir (mantle residuum)
831 would be characterized by higher $^3\text{He}/^4\text{He}$ than both partial melt and undegassed mantle, because it
832 is characterized by lower (Th+U)/He ratios (black dot 1 in Fig. 8b). The petrological implications
833 for this alternative model are particularly relevant. $^3\text{He}/^4\text{He}$ values as high as 50 R/Ra would reflect
834 not primitive (undegassed) mantle sources but derivation from depleted residua (Parman et al.,
835 2005). Partial melting effectively cannot decrease He/(Th+U) ratios in the mantle residuum and
836 high He/(Th+U) ratios can develop in mantle residua through large extents of melting, but at the
837 same time are associated with low He (and other noble gases) concentrations (Jackson et al., 2013).

838 In conclusion both high and low $^3\text{He}/^4\text{He}$ ratios can be associated with recycling processes. Low
839 $^3\text{He}/^4\text{He}$ requires the presence of an old U+Th-rich component (e.g., recycled crust or sediment),
840 while high $^3\text{He}/^4\text{He}$ ratios can be explained by recycling of refractory peridotite or olivine-rich
841 cumulates (rich in gas-filled bubbles or cracks; e.g., Natland, 2003; Anderson, 2007). In either case
842 recycling down to the lower mantle is not required.

843

844 **4. Ink cartridges in the mantle isotopic printer**

845 $^{87}\text{Sr}/^{86}\text{Sr}$ ratios of HiMu- and HiMu-like-OIB are all lower than BSE. This characteristic is at odds
846 with derivation from a primitive (i.e., never tapped by basaltic extraction) source. This conundrum

847 has been explained by derivation from a deep mantle source that interacted with low- $^{87}\text{Sr}/^{86}\text{Sr}$
848 recycled oceanic crust (e.g., Hofmann, 1997, 2003). The low $^{87}\text{Sr}/^{86}\text{Sr}$ characteristic is intrinsic of a
849 partial melt generated from a depleted (DMM) source in which Rb, more incompatible than Sr
850 during melt extraction, is preferentially transferred to the melt. If such a depleted, low Rb/Sr source
851 partially melts again, the new liquid is characterized by low $^{87}\text{Rb}/^{86}\text{Sr}$, and consequentially evolves
852 towards low $^{87}\text{Sr}/^{86}\text{Sr}$ isotopic ratios. Low Rb has also been postulated as a consequence of
853 hydrothermal alteration of oceanic crust that concentrates this metal in secondary veins that are
854 easily mobilized during the first stages of dehydration metamorphic reaction occurring at shallow
855 depths below the supra-subduction lithospheric mantle wedge (e.g., Chauvel et al., 1992).

856 Ancient recycling (of the order of 2 Gyr and more) of MORB-like lithologies (characterized by
857 low-to-very-low Rb/Sr and thus low-to-very-low $^{87}\text{Sr}/^{86}\text{Sr}$) would have reduced the $^{87}\text{Sr}/^{86}\text{Sr}$ of the
858 primitive deep mantle from BSE to values indistinguishable from present-day MORB.

859 The EMI-EMII OIB $^{87}\text{Sr}/^{86}\text{Sr}$ ratios higher than BSE have been explained by derivation from a
860 deep mantle that interacted with high $^{87}\text{Sr}/^{86}\text{Sr}$ lithologies in the form of subducted sediments
861 (pelitic and terrigenous) and delaminated/eroded lower continental crust (e.g., Zindler and Hart,
862 1986; Lustrino and Dallai, 2003; Stracke et al., 2005; Jackson and Dasgupta, 2008; Willbold and
863 Stracke, 2010; Stracke, 2012). What is interesting is that in some cases (e.g., HiMu-like basalts) the
864 contribution of “normal” oceanic crust is dominant (low $^{87}\text{Sr}/^{86}\text{Sr}$) compared to the geochemical
865 (and isotopic) budget of altered oceanic crust (characterized by much higher Rb/Sr ratios) or the
866 thin sediment veneer (e.g., White, 2010; Stracke, 2012). In all these three cases, the HiMu, EMI and
867 EMII components (actually isotopic “flavours”) provide evidence of variable interaction with a
868 shallow DMM-like mantle, producing the various “colors” recorded in intra-plate oceanic basalts.

869 In summary, the isotopic compositions of three of the main four “ink cartridges” of the mantle
870 isotopic printer (HiMu, EMI and EMII) are essentially related to recycling of subducted lithologies
871 (fresh vs. altered oceanic crust, pelitic vs. terrigenous sediments, plus variable contribution of
872 metasomatically modified oceanic lithospheric mantle) or tectonic erosion of the base of the supra-
873 subduction continental mantle wedge (e.g., Clift and Vannucchi, 2004; Willbold and Stracke, 2010).
874 Alternative but similar views interpret these three “colors” as partial melts or ancient gases frozen
875 in the shallow boundary layer (e.g., Natland, 2003; Anderson, 2007; Niu et al., 2011; Pilet et al.,
876 2011; Pilet, 2014). These interpretations, albeit with several necessary distinctions and case-by-case
877 peculiarities, are valid. The models explaining the significance of the geochemical mantle zoo

878 (Stracke et al., 2005) can be grouped into two categories. One considers that the most peculiar
879 isotopic characteristics of the mantle end-members reflect recycling (both directly, in the form of
880 subducted lithologies, or indirectly, in the form of tectonically eroded lithospheric sole) of material
881 once stored at shallow depths or at the Earth's surface (e.g., Hofmann, 2003; White, 2010; Stracke,
882 2012). The second considers that Na-K-H-C-rich partial melts infiltrating the shallow mantle can
883 metasomatize the lithospheric mantle and are not necessarily related to subduction tectonics (e.g.,
884 Niu and O'Hara, 2008; Pilet, 2014). Whichever is correct, the isotope systematics do not require
885 deep mantle sources nor temperature excesses. This means that any mantle plume hypothesis based
886 on geochemical arguments is fundamentally unsafe.

887 According to the standard geochemical model, the isotopic cartridges of the mantle printer are in
888 the deepest mantle because this is the only place not involved in vigorous convection (Fig. 1b). The
889 peculiar isotopic characteristics of the various mantle end-members are explained by isolation from
890 convection. This need for isolation actually applies more to the MORB source than to hypothetical
891 plume sources. What would be the difference if the recycled lithologies are stored not in the deeper
892 mantle, but in the upper thermal boundary layer (D" Fig. 1b, also known as Perisphere or LLAMA)?
893 There would be no difference at all. Having four ink cartridges close to the Earth's surface in the
894 shallowest mantle and the TZ also has the advantage that there is then no need to assume the
895 thermal state, chemical composition and rheological behaviour of the deep mantle, for which there
896 is little supporting evidence. Because of the low temperatures and high strength at the top of the
897 upper boundary layer, ionic diffusivities are very low and even ancient He isotope signatures can be
898 preserved.

899 What is necessary in the geochemical mantle plume model is the presence of regions in the Earth's
900 interior that escape continuous homogenization. In order to allow a given isotopic ratio to grow, the
901 source (isotopic color) must be placed somewhere (ink cartridge) and reside there until it is tapped.
902 Three of the four ink cartridges (as identified by different isotopic systematics) can certainly be
903 placed in the upper 150-250 km of the mantle.

904 As concerns the volume of magma production associated with postulated mantle plumes, it is
905 sufficient to consider the following. Assuming the presence of only 2% melt in a 100 km-thick
906 seismic Low Velocity Zone (e.g., the LLAMA volume of Anderson, 2011), the estimated amount of
907 melt there is of the order of 10^9 km³. This amount is ample to explain the volumes erupted in

908 typical OIB or Large Igneous Province eruptions (e.g., Mahoney and Mahoney, 1997; Cañón-Tapia,
909 2010).

910

911 **5. Concluding remarks**

912 Various petrogenetic models have been proposed to explain the presence, the abundance, the
913 physical state and the origin of the four principal mantle end-members (DMM, HiMu, EMI and
914 EMII) in the oceanic mantle. These end-members, based on Sr-Nd-Pb isotope systematics represent
915 the most extreme compositions that can be found in the oceanic mantle. Extreme values
916 occasionally found in magmas emplaced in continental settings can be related to interaction of
917 mantle partial melts with isotopically extreme crustal lithologies.

918 We interpret these end-members using the analogy of printing, where four basic colors (black, red,
919 magenta, yellow), mixed in the appropriate amounts, can produce the full range of colors. Similarly,
920 assuming four isotopic mantle end-members, it is possible to produce the whole range of oceanic
921 basalt isotopic compositions. All the “colors” are present in a relatively restricted area east of
922 Australia, in the Polynesia-Melanesia-Micronesia region. In some cases they are virtually present in
923 the same volcanic district (e.g., Jackson et al., 2014), rendering the possibility of a provenance from
924 the D" Region (without complete mixing of the “colors”) at least dubious. With the exception of
925 DMM, all the other mantle end-members require the involvement of olivine-poor lithologies. These
926 lithologies have been identified in upper/lower crustal rocks, recycled oceanic crust, terrigenous
927 and/or pelagic sediments, kimberlites, carbonatites, sulphides, oxides or frozen basaltic melts
928 crystallized at depth (e.g., Ivanov, in press; Pilet, in press; Smith, in press).

929 Geochemists and petrologists now generally agree on the origin of these colors. The great
930 differences in opinion lie in where the “isotopic cartridges” are considered to be located in the
931 Earth’s interior. Thermal anomalies are not associated with these end-members, nor are they
932 required in any form. A small degree of melting is sometimes invoked to explain absolute trace
933 element contents or the trace element fractionation recorded in lavas. Shallow degassing and
934 contamination is implied in noble gas systematics. Helium isotopes cannot be used to constrain the
935 existence of an undegassed lower mantle or the physical conditions of deep mantle upwellings.
936 Extensive overlap of MORB and OIB in terms of Sr-Nd isotopic ratios and nearly complete overlap
937 in Pb isotopes indicate that the mantle sources are not necessarily very different in terms of depth or
938 insulated from each other.

939 Shallow anomalies are responsible for intra-plate volcanism. Mantle plumes and a fully
940 convecting mantle are unproven assumptions. Physically realistic Earth models have a thick upper
941 thermal boundary layer, characterized by superadiabatic thermal gradient, with a thickness of the
942 order of 100-200 km. Three out of the four mantle “colors” (HiMu, EMI and EMII) can be drawn
943 from this region of the Earth, which is also mobilised by shallow convection associated with plate
944 tectonics. The fourth color, by far the most abundant, is represented by DMM probably comprises
945 the shallow mantle matrix or, as recently proposed, passively updraft mantle from the TZ (Anderson
946 and Natland, 2014). This thermodynamically self-consistent model eliminates the need for lower-
947 mantle involvement in oceanic basalt petrogenesis and surface igneous activity in general. All the
948 isotopic color cartridges can be placed at shallow depths and tapping of lower mantle is not
949 required.

950

951 **Acknowledgements**

952 Don passed away during the corrections of the last draft of this manuscript. It is an immense
953 honour for me to have had the possibility to co-author a paper with such a giant of the Earth
954 Sciences. This manuscript is dedicated to Democritus (V century B.C.), considered the father of the
955 modern science. This ancient Greek philosopher understood the atomistic nature of matter and spent
956 his life fighting dogma. For this reason, more than 99% of his products have been lost, destroyed by
957 religious communities. The Democritus philosophical approach luckily survived, at least partially,
958 in the ancient Greek philosopher Epicurus (III century B.C.), and, above all, the great Latin poem
959 "*De Rerum Natura*" of Lucretius (I century B.C.). I find that the love for the truth, the obstinate hate
960 against dogma and the genius constitute solid connecting lines between Democritus and Don
961 Anderson.

962 ML thanks MIUR PRIN (2010 20107ESMX9_001) and Ateneo La Sapienza (Fondi Ateneo 2012,
963 2013) for financial support. ML greatly enjoyed discussions with the MP group, and use of the
964 website www.mantleplumes.org. Gillian Foulger is warmly thanked for the detailed comments,
965 suggestions and the punctual English text sharpening process on several draft versions. Detailed
966 reviews by Marjorie Wilson (Leeds, UK) and Erin Beutel (Charleston, USA) improved the quality
967 of the manuscript.

968

969

970 **References**

- 971 Allègre, C.J., 1969, Comportement des systems U-Th-Pb dans le manteau supérieur et modèle
972 d'évolution de cedernier au cours des temps géologiques: *Earth and Planetary Science Letters*, v.
973 5, p. 261-269.
- 974 Anderson, D.L., 1989, Where on Earth is the crust?: *Physics Today*, v. 42, p. 38-46.
- 975 Anderson, D.L., 1995, Lithosphere, asthenosphere, and perisphere: *Reviews of Geophysics*, v. 33,
976 p. 125-149.
- 977 Anderson, D.L., 1998, The helium paradoxes: *Proceedings of the National Academy of Sciences*, v.
978 95, p. 4822-4827.
- 979 Anderson, D.L., 2007, *New Theory of the Earth*: Cambridge Univ. Press, 384 pp.
- 980 Anderson, D.L., 2011, Hawaii, boundary layers and ambient mantle – Geophysical constraints:
981 *Journal of Petrology*, v. 52, p. 1547-1577.
- 982 Anderson, D.L., 2013, The persistent mantle plume myth: *Australian Journal of Earth Sciences*, v.
983 60, p. 657-673.
- 984 Anderson, D.L., and King, S.D., 2014, Driving the Earth machine?: *Science*, v. 346, p. 1184-1185.
- 985 Anderson, D.L., and Natland, J.H., 2014, Mantle updrafts and mechanisms of oceanic volcanism:
986 *Proceedings of the National Academy of Sciences*, v. 111, p. E4298-E4304.
- 987 Ballentine, C.J., 2012, A dash of deep nebula on the rocks: *Nature*, v. 486, p. 40-41.
- 988 Ballmer, M.D., Ito, G., Wolfe, C.J., and Solomon, S.C., 2013, Double layering of a thermochemical
989 plume in the upper mantle beneath Hawaii: *Earth and Planetary Science Letters*, v. 376, p. 155-
990 164.
- 991 Bolhar, R., Kamber, B.S., and Collerson, K.D., 2007, U-Th-Pb fractionation in Archaean lower
992 continental crust: implications for terrestrial Pb isotope systematics: *Earth and Planetary Science*
993 *Letters*, v. 254, p. 127-145.
- 994 Borisova, A.Yu., Belyatsky, B.V., Portnyagin, M.V., and Sushchevskaya, N.M., 2001, Petrogenesis
995 of olivine-phyric basalts from the Aphanasey-Nikitin Rise: evidence for contamination by
996 cratonic lower continental crust: *Journal of Petrology*, v. 42, p. 277-319.
- 997 Bull, A.L., Domeier, M., and Torsvik, T.H., 2014, The effect of plate motion history on the
998 longevity of deep mantle heterogeneities: *Earth and Planetary Science Letters*, v. 401, p. 172-
999 182.

1000 Cadoux, A., Blichert-Toft, J., Pinti, D.L., and Albarède, F., 2007, A unique lower mantle source for
1001 southern Italy volcanics: *Earth and Planetary Science Letters*, v. 259, p. 227-238.

1002 Camp, V.E., 2013, Origin of Columbia River Basalt: Passive rise of shallow mantle or active
1003 upwelling of a deep-mantle plume? In: Reidel, S.P., Camp, V.E., Ross, M.E., Wolff, J.A.,
1004 Martin, B.S., Tolán, T.L., and Wells, R.E. (Eds.): *The Columbia River Flood Basalt Province:*
1005 *Geological Society of America Special Paper*, v. 497, p. 181-199.

1006 Cañón-Tapia, E., 2010, Origin of large igneous provinces: the importance of a definition:
1007 *Geological Society of America Special Paper*, v. 470, p. 77-101.

1008 Caro, G., and Bourdon, B., 2010, Non-chondritic Sm/Nd ratio in the terrestrial planets:
1009 consequences for the geochemical evolution of the mantle-crust system: *Geochimica et*
1010 *Cosmochimica Acta*, v. 74, p. 3333-3349.

1011 Chauvel, C., Goldstein, S.L., and Hofmann, A.W., 1995, Hydration and dehydration of oceanic
1012 crust controls Pb evolution of the mantle: *Chemical Geology*, v. 126, p. 65-75.

1013 Chauvel, C., Hofmann, A.W., and Vidal, P., 1992, HIMU-EM: the French Polynesian connection:
1014 *Earth and Planetary Science Letters*, v. 110, p. 99-119.

1015 Campbell, I.H., and Griffiths, R.W., 2014, Did the formation of D" cause the Archean-Proterozoic
1016 transition?: *Earth and Planetary Science Letters*, v. 388, p. 1-8.

1017 Chauvel, C., Goldstein, S.L., and Hofmann, A.W., 1995, Hydration and dehydration of oceanic
1018 crust controls Pb evolution in the mantle: *Chemical Geology*, v. 126, p. 65-75.

1019 Class, C., and Goldstein, S.L., 2005, Evolution of helium isotopes in the Earth's mantle: *Nature*, v.
1020 436, p. 1107-1112.

1021 Clift, P.D., and Vannucchi, P., 2004, Controls on the tectonic accretion versus erosion in subduction
1022 zones: implications for the origin and recycling of the continental crust: *Reviews of Geophysics*,
1023 v. 42, RG2001, 2003RG000127.

1024 Cloetingh, S., Burov, E., and Francois, T., 2013, Thermo-mechanical controls on intra-plate
1025 deformation and the role of plume-folding interactions in continental topography: *Gondwana*
1026 *Research*, v. 24, p. 815-837.

1027 Davies, G.F., 2011, *Mantle convection for geologists*: Cambridge Univ. Press, 232 pp.

1028 Dupré, B., and Allègre, C.J., 1983, Pb–Sr isotope variation in Indian Ocean and mixing phenomena:
1029 *Nature*, v. 303, p. 142-146.

1030 Faccenna, C., Becker, Shaping mobile belts by small-scale convection, *Nature*, v. 465, p. 602-605.

- 1031 Farnetani, C.G., and Richards, M.A., 1994, Numerical investigation of the mantle plume initiation
1032 model for flood basalt events: *Journal of Geophysical Research*, v. 99, p. 13813-13883.
- 1033 Faure, G., and Powell, J.L., 1972, *Strontium isotope geology*: Springer Verlag, Berlin, 188 pp.
- 1034 Fedele, L., Lustrino, M., Melluso, L., Morra, V., Zanetti, A., and Vannucci, R., 2015, Trace-
1035 element partitioning between plagioclase, alkali feldspar, Ti-magnetite, biotite, apatite and
1036 evolved potassic liquids from Campi Flegrei (Southern Italy): *American Mineralogist*, v. 100, p.
1037 233-249.
- 1038 Foulger, G.R., 2010, *Plates vs. plumes: A geological controversy*. Wiley-Blackwell 328 pp.
- 1039 Foulger, G.R., Panza, G.F., Artemieva, I.M., Bastow, I.D., Cammarano, F., Evans, J.R., Hamilton,
1040 W.B., Julian, B.R., Lustrino, M., Thybo, H., and Yanovskaya, T.B., 2013, Caveats on
1041 tomographic images: *Terra Nova*, v. 25, p. 259-281.
- 1042 Fulla, J., Afonso, J.C., Connolly, J.A.D., Fernandez, M., Garcia-Castellanos, D., and Zeyen, H.,
1043 2009, LitMod3D: an interactive 3-D software to model the thermal, compositional, density,
1044 seismological and rheological structure of the lithosphere and sublithospheric upper mantle:
1045 *Geochemistry Geophysics and Geosystems*, Q08019, doi:10.1029/2009GC002391.
- 1046 Gast, P.W., 1960, Limitations on the composition of the upper mantle: *Journal of Geophysical*
1047 *Research*, v. 65, p. 1287-1297.
- 1048 Gast, P.W., 1968, Trace element fractionation and the origin of tholeiitic and alkaline magma types:
1049 *Geochimica et Cosmochimica Acta*, v. 32, p. 1057-1086.
- 1050 Glisovic, P., and Forte, A.M., 2014, Reconstructing the Cenozoic evolution of the mantle:
1051 implications for mantle plume dynamics under the Pacific and Indian plates: *Earth and Planetary*
1052 *Science Letters*, v. 390, p. 146-156.
- 1053 Gonnermann, H.M., and Mukhopadhyay, S., 2009, Preserving noble gases in a convecting mantle:
1054 *Nature*, v. 459, p. 560-563.
- 1055 Graham, D.W., Hanan, B.B., Hémond, C., Blichert-Toft, J., and Albarède, F., 2014, Helium
1056 isotopic textures in Earth's upper mantle: *Geochemistry Geophysics and Geosystems*, v. 15, p.
1057 2048-2074.
- 1058 Graham, D.W., Larsen, L.M., Hanan, B.B., Storey, M., Pedersen, A.K., and Lupton, J.E., 1998,
1059 Helium isotope composition of the early Iceland mantle plume inferred from the Tertiary picrites
1060 of West Greenland: *Earth and Planetary Science Letters*, v. 160, p. 241-255.

1061 Green, D.H., Hibberson, W.O., Kovacs, I., and Rosenthal, A., 2010, Water and its influence on the
1062 lithosphere-asthenosphere boundary: *Nature*, v. 467, p. 448-451.

1063 Griffiths, R.W., and Campbell, I.H., 1990, Stirring and structure in mantle starting plumes: *Earth
1064 and Planetary Science Letters*, v. 99, p. 66-78.

1065 Gudfinnsson, G.H., and Presnall, D.C., 2005, Continuous gradations among primary carbonatitic,
1066 kimberlitic, melilitic, basaltic, picritic, and komatiitic melts in equilibrium with garnet lherzolite
1067 at 3-8 GPa: *Journal of Petrology*, v. 46, p. 1645-1659.

1068 Gutenberg, B., 1959, Wave velocities below the Mohorovicic discontinuity: *Geophysical Journal of
1069 the Royal Astronomical Society*, v. 2, p. 348-352.

1070 Hanyu, T., 2014, Deep plume origin of the Louisville hotspot: noble gas evidence: *Geochemistry
1071 Geophysics and Geosystems*, v. 15, p. 565-576.

1072 Hanyu, T., Dosso, L., Ishizuka, O., Tani, K., Hanan, B.B., Adam, C., Nakai, S., Senda, R., Chang,
1073 Q., and Tatsumi, Y., 2013, Geochemical diversity in submarine HIMU basalts from Austral
1074 Islands, French Polynesia: *Contributions to Mineralogy Petrology*, v. 166, p. 1285-1304.

1075 Hanyu, T., Kawabata, H., Tatsumi, Y., Kimura, J.-I., Hyodo, H., Sato, K., Miyazaki, T., Chang, Q.,
1076 Hirahara, Y., Takahashi, T., Senda, R., and Nakai, S., 2014, Isotope evolution in the HIMU
1077 reservoir beneath St. Helena: implications for the mantle recycling of U and Th: *Geochimica et
1078 Cosmochimica Acta*, v. 143, p. 232-252.

1079 Hart, S.R., 1984, A large-scale isotope anomaly in the Southern Hemisphere mantle: *Nature*, v. 309,
1080 p. 753-757.

1081 Hart, S.R., 2014, Geochemical diversity of the mantle: 50 years of acronyms. AGU Fall Meeting,
1082 San Francisco, V22-B01.

1083 Hanyu, T., Clague, D.A., Kaneoka, I., Dunai, T.J., and Davies, G.R., 2005, Noble gas systematics
1084 of submarine alkalic lavas near the Hawaiian hotspot: *Chemical Geology*, v. 214, p. 135-155.

1085 Herzberg, C., 2011, Basalts as temperature probes of the Earth's mantle. *Geology*, v. 39, p. 1179-
1086 1180.

1087 Hirschmann, M.M., and Dasgupta, R., 2009, The H/C ratio of Earth's near surface and deep
1088 reservoirs, and consequences for deep Earth volatile cycles: *Chemical Geology*, v. 262, p. 4-16.

1089 Hofmann, A.W., 1997, Mantle geochemistry: the message from oceanic volcanism: *Nature*, v. 385,
1090 p. 219-229.

1091 Hofmann, A.W., 2003, Sampling mantle heterogeneity through oceanic basalts: Isotopes and trace
1092 elements: In R.W. Carlson, Holland, H.D., and Turekian, K.K., (Eds.). Treatise on
1093 Geochemistry: The Mantle and Core, p. 61-101.

1094 Hofmann, A.W., 2014, Fifty-one years of Hawaiian hotspot debate. AGU Fall Meeting, San
1095 Francisco, V23G-01.

1096 Huang, S., Frey, F.A., 2005, Recycled oceanic crust in the Hawaiian plume: evidence from
1097 temporal geochemical variations within the Koolau shield: Contributions to Mineralogy and
1098 Petrology, v. 149, p. 556-575.

1099 Humphreys, E., Schmandt, B., 2011, Looking for mantle plumes: Physics Today, v. 64, p. 34-39.

1100 Ivanov, A.V., in press, Why volatiles are required for cratonic flood basalt volcanism: two
1101 examples from the Siberian Craton: In: G.R. Foulger, M. Lustrino and S.D. King (Eds.) Volume
1102 in honour of Don L. Anderson.

1103 Jackson, C.R.M., Parman, S.W., Kelley, S.P., and Cooper, R.F., 2013, Constraints on light noble
1104 gas partitioning at the conditions of spinel-peridotite melting: Earth and Planetary Science
1105 Letters, v. 384, p. 178-187.

1106 Jackson, M.G., Carlson, R.W., Kurz, M.D., Kempton, P.D., Francis, D., and Blusztajn, J., 2010,
1107 Evidence for the survival of the oldest terrestrial mantle reservoir: Nature, v. 466, p. 853-856.

1108 Jackson, M.G., and Dasgupta, R., 2008, Compositions of HIMU, EM1, and EM2 from global trends
1109 between radiogenic isotopes and major elements in oceanic island basalts: Earth and Planetary
1110 Science Letters, v. 276, p. 175-186.

1111 Jackson, M.G., Hart, S.R., Konter, J.G., Kurz, M.D., Blusztajn, J., and Farley, K.A., 2014, Helium
1112 and lead isotopes reveal the geochemical geometry of the Samoan plume: Nature, v. 514, p. 355-
1113 358.

1114 Jackson, M.G., and Jellinek, A.M., 2013, Major and trace element composition of the high $^3\text{He}/^4\text{He}$
1115 mantle: implications for the composition of a nonchondritic Earth: Geochemistry Geophysics
1116 and Geosystems, v. 14, doi: 10.1002/ggge.20188

1117 Kawabata, H., Hanyu, T., Chang, Q., Kimura, J.-I., Nichols, A.R.L., and Tatsumi, Y., 2011, The
1118 petrology and geochemistry of St. Helena alkali basalts: evaluation of the oceanic crust-recycling
1119 model for HIMU OIB: Journal of Petrology, v. 52, p. 791-838.

1120 Kawakatsu, H., Kumar, P., Takei, Y., Shinohara, M., Kanazawa, T., Araki, E., and Suyehiro, K.,
1121 2009, Seismic evidence for sharp lithosphere-asthenosphere boundaries of oceanic plates:
1122 Science, v. 324, p. 499-502.

1123 Keiding, J.K., Trumbull, R.B., Veksler, I.V., and Jerram, D.A., 2011, On the significance of ultra-
1124 magnesian olivines in basaltic rocks: Geology, v. 39, p. 1095-1098.

1125 Keshav, S., Gudfinnsson, G.H., 2014, Melting phase equilibria of model carbonated peridotite from
1126 8 to 12 GPa in the system CaO-MgO-Al₂O₃-SiO₂-CO₂ and kimberlitic liquids in the Earth's
1127 upper mantle: American Mineralogists, v. 99, p. 1119-1126.

1128 Lee, W.-J., Huang, W.L., and Wyllie, P., 2000, Melts in the mantle modeled in the system CaO-
1129 MgO-SiO₂-CO₂ at 2.7 GPa: Contributions to Mineralogy and Petrology, v. 138, p. 199-231.

1130 Li, M., McNamara, A.K., and Garnero, E.J., 2014, Chemical complexity of hotspots caused by
1131 cycling oceanic crust through mantle reservoirs: Nature Geosciences, v. 7, p. 366-370.

1132 Litasov, K.D, and Ohtani, E., 2003, Stability of various hydrous phases in CMAS pyrolite-H₂O
1133 system up to 25 GPa: Physics and Chemistry Of Minerals, v. 30, p. 147-156.

1134 Litasov, K.D., 2011, Physicochemical conditions for melting in the Earth's mantle containing a C-
1135 O-H fluid (from experimental data): Russian Geology and Geophysics, v. 52, p. 475-492.

1136 Lustrino, M., 2005, How the delamination and detachment of lower crust can influence basaltic
1137 magmatism: Earth-Science Reviews, v. 72, p. 21-38.

1138 Lustrino, M., 2011, What 'anorogenic' igneous rocks can tell us about the chemical composition of
1139 the upper mantle: case studies from the circum-Mediterranean area: Geological Magazine, v.
1140 148, p. 304-316.

1141 Lustrino, M., and Dallai L., 2003, On the origin of EM-I end-member: Neues Jahrbuch fur
1142 Mineralogie. Abhandlungen, v. 179, p. 85-100.

1143 Lustrino, M., and Wilson, M., 2007, The Circum-Mediterranean Anorogenic Igneous Province:
1144 Earth-Science Reviews, v. 81, p. 1-65.

1145 Lyubetskaya, T., and Korenaga, J., 2007, Chemical composition of Earth's primitive mantle and its
1146 variance: 1. Methods and results: Journal of Geophysical Research, v. 112, B03211,
1147 doi:10.1029/2005JB004223.

1148 Mahoney, J.J., and Coffin, M.F., (Eds), 1997, Large igneous provinces. Continental, oceanic and
1149 planetary flood volcanism: American Geophysical Union Geophysical Monograph, v. 100, 438
1150 pp.

1151 Mahoney, J.J., White, W.M., Upton, B.G.J., Neal, C.R., and Scrutton, R.A., 1996, Beyond EM-1:
1152 lavas from Afanasy-Nikitin Rise and the Crozet Archipelago, Indian Ocean: *Geology*, v. 24, p.
1153 615-618.

1154 Mallik, A., and Dasgupta, R., 2014, Effect of variable CO₂ on eclogite-derived andesite and
1155 lherzolite reaction at 3 GPa – implications for mantle source characteristics of alkalic island
1156 basalts: *Geochemistry Geophysics and Geosystems*, v. 15, p. 1533-1557.
1157 doi:10.1002/2014GC005251

1158 McKenzie, D., and Bickle, M.J., 1988, The volume and composition of melt generated by extension
1159 of the lithosphere: *Journal of Petrology*, v. 29, p. 625-679.

1160 Meibom, A., Anderson, D.L., Sleep, N.H., Frei, R., Page Chamberlain, C., Hren, M.T., and
1161 Wooden, J.L., 2003, Are high ³He/⁴He ratios in oceanic basalts an indicator of deep-mantle
1162 plume components?: *Earth and Planetary Science Letters*, v. 208, p. 197-204.

1163 Merle, R., Jourdan, F., Marzoli, A., Renne, P.R., Grange, M., and Girardeau, J., 2009, Evidence of
1164 multi-phase Cretaceous to Quaternary alkaline magmatism on Tore-Madeira Rise and
1165 neighbouring seamounts from ⁴⁰Ar/³⁹Ar ages: *Journal of the Geological Society of London*, v.
1166 166, p. 879-894.

1167 Montelli, R., Nolet, G., Dahlen, F.A., Masters, G., Engdahl, R., Hung, S.-H., 2004. Finite-frequency
1168 tomography reveals a variety of plumes in the mantle: *Science*, v. 303, p. 338-343.

1169 Moreira, M., Kanzari, A., and Madureira, P., 2012, Helium and neon isotopes in Sao Miguel island
1170 basalts, Azores archipelago: new constraints on the “low ³He” hotspot origin: *Chemical*
1171 *Geology*, v. 322-323, p. 91-98.

1172 Morgan, W.J., 1971, Convection plumes in the lower mantle: *Nature*, v. 230, p.42-43.

1173 Morgan, W.J., 1972, Deep mantle convection plumes and plate motions: *American Association of*
1174 *Petroleum Geologists Bulletin*, v. 56, p. 203-213.

1175 Mourao, C., Moreira, M., Mata, J., Raquin, A., and Madeira, J., 2012, Primary and secondary
1176 processes constraining the noble gas isotopic signatures of carbonatites and silicate rocks from
1177 Brava Island: evidence for a lower mantle origin of the Cape Verde plume: *Contributions to*
1178 *Mineralogy and Petrology*, v. 163, p. 995-1009.

1179 Nakagawa, T., and Tackley, P.J., 2014. Influence of combined primordial layering and recycled
1180 MORB on the coupled thermal evolution of Earth’s mantle and core: *Geochemistry Geophysics*
1181 *and Geosystems*, v. 15, p. 619–633, doi:10.1002/2013GC005128.

1182 Natland, J.H., 2003. Capture of helium and other volatiles during the growth of olivine phenocrysts
1183 in picritic basalts from the Juan Fernandez Islands: *Journal of Petrology*, v. 44, p. 421-456.

1184 Niu, Y., and O'Hara, M.J., 2008, Global correlations of ocean ridge basalt chemistry with axial
1185 depth: a new perspective: *Journal of Petrology*, v. 49, p. 633-664.

1186 Niu, Y., Wilson, M., Humphreys, E.R., and O'Hara, M.J., 2011, The origin of intra-plate island
1187 basalt (OIB): the lid effect and its geodynamic implications: *Journal of Petrology*, v. 52, p. 1443-
1188 1468.

1189 Nixon, P.H., (Ed.), 1987, *Mantle xenoliths*: John Wiley & Sons Ltd. 864 pp.

1190 Ozima, M., and Igarashi, G., 2000, The primordial noble gases in the Earth: a key constraint on
1191 Earth evolution models: *Earth and Planetary Science Letters*, v.176, p. 219-232.

1192 Parman, S.W., Kurz, M.D., Hart, S.R., and Grove, T.L., 2005, Helium solubility in olivine and
1193 implications for high $^3\text{He}/^4\text{He}$ in ocean island basalt: *Nature*, v. 437, p. 1140-1143.

1194 Pearson, D.G., Brenker, F.E., Nestola, F., McNeill, J., Nasdala, L., Hutchison, M.T., Matveev, S.,
1195 Mather, K., Silversmit, G., Schmitz, S., Vekemans, B., and Vincze, L., 2014, Hydrous mantle
1196 transition zone indicated by ringwoodite included within diamond: *Nature*, v. 507, p. 221-224.

1197 Peters, B.J., Day, J.M.D., 2014, Assessment of relative Ti, Ta and Nb (TITAN) enrichments in
1198 ocean island basalts: *Geochemistry Gophysics and Geosystems*, v. 15, doi:
1199 10.1002/2014GC005506.

1200 Pfander, J.A., Jung, S., Münker, C., Stracke, A., and Mezger, K., 2012, A possible high Nb/Ta
1201 reservoir in the continental lithospheric mantle and consequences on the global Nb budget –
1202 evidence from continental basalts from central Germany: *Geochimica et Cosmochimica Acta*, v.
1203 77, p. 232-251.

1204 Pilet, S., 2014, Generation of low-silica alkaline lavas: petrological constraints, models and thermal
1205 implications: In: G.R. Foulger, M. Lustrino and S.D. King (Eds.) Volume in honour of Don L.
1206 Anderson.

1207 Pilet, S., Baker, M.B., Müntener, O., Stolper, E.M., 2011, Monte Carlo simulations of metasomatic
1208 enrichment in the lithosphere and implications for the source of alkaline basalts: *Journal of*
1209 *Petrology*, v. 52, p. 1415-1452.

1210 Plank, T., 2014, The chemical composition of subducting sediments. *Treatise on Geochemistry* (2nd
1211 edition), In: R. Rudnick (Ed.) *Treatise on Geochemistry*, Vol. 4: The crust, 607-629.

1212 Prelevic, D., and Foley, S.F., 2007, Accretion of arc-oceanic lithospheric mantle in the
1213 Mediterranean: evidence from extremely high-Mg olivines and Cr-rich spinel inclusions in
1214 lamproites: *Earth and Planetary Science Letters*, v. 256, p. 120-135.

1215 Putirka, K.D., 2005, Mantle potential temperatures at Hawaii, Iceland, and the mid-ocean ridge
1216 system, as inferred from olivine phenocrysts: evidence for thermally driven mantle plumes:
1217 *Geochemistry Geophysics and Geosystems*, v. 6, Q05L08. doi:10.1029/2005GC000915.

1218 Ringwood, A.E., 1979, *Composition and origin of the Earth*. Springer Verlag, New York, 295 pp.

1219 Salters, V.J.M., Sachi-Kocher, A., 2010, An ancient metasomatic source for the Walvis Ridge
1220 basalts: *Chemical Geology*, v. 273, p. 151-167.

1221 Sandwell, D.T., Muller, R.D., Smith, W.H.F., Garcia, E., and Francis, R., 2014, New global marine
1222 gravity model from Cryosat-2 and Jason-1 reveals buried tectonic structure. *Science*, 346, 65-67.

1223 Schmidt, M.W., and Poli S., 2014, Devolatilization during subduction. In: R. Rudnick (Ed.) *Treatise*
1224 *on Geochemistry*, Vol. 4: The crust, 669-701.

1225 Schuberth, B.S.A., and Bunge, H.-P., 2009, Thermal versus elastic heterogeneity in high-resolution
1226 mantle circulation models with pyrolite composition: high plume excess temperatures in the
1227 lowermost mantle: *Geochemistry Geophysics and Geosystems*, v. 10, Q01W01,
1228 doi:10.1029/2008GC002235.

1229 Smith, A.D., in press, A Perisphere/LLAMA model for Hawaiian volcanism: In: G.R. Foulger, M.
1230 Lustrino and S.D. King (Eds.) *Volume in honour of Don L. Anderson*.

1231 Sobolev, S.V., Sobolev, A.V., Kuzmin, D.V., Krivolutsкая, N.A., Petrunin, A.G., Arndt, N.T.,
1232 Radko, V.A., and Vasiliev, Y.R., 2011, Linking mantle plumes, large igneous provinces and
1233 environmental catastrophes: *Nature*, v. 477, p. 312-316.

1234 Stracke, A., 2012, Earth's heterogeneous mantle: a product of convection-driven interaction
1235 between crust and mantle: *Chemical Geology*, v. 330-331, p. 274-299.

1236 Stracke, A., Hofmann, A.W., and Hart S.R., 2005, FOZO, HIMU and the rest of the mantle zoo:
1237 *Geochemistry Geophysics and Geosystems*, v. 6, Q05007. DOI: 10.1029/2004GC000824.

1238 Stuart, F.M., Lass-Evans, S., Fitton, J.G., and Ellam, R.M., 2003, High $^3\text{He}/^4\text{He}$ ratios in picritic
1239 basalts from Baffin Island and the role of a mixed reservoir in mantle plumes: *Nature*, v. 424, p.
1240 57-59.

1241 Tanaka, R., Nakamura, E., and Takahashi, E., 2002, Geochemical evolution of Koolau Volcano,
1242 Hawaii: *AGU Geophys. Monograph*, v. 128, p. 311-332.

- 1243 Tatsumoto, M., 1978, Isotopic composition of lead in oceanic basalt and its implication to mantle
1244 evolution: *Earth and Planetary Science Letters*, v. 38, p. 63-87.
- 1245 Vitale Brovarone, A., and Beyssac, O., 2014, Lawsonite metasomatism: a new route for water to the
1246 deep Earth: *Earth and Planetary Science Letters*, v. 393, p. 275-284.
- 1247 White, W.M., 2010, Oceanic island basalts and mantle plumes: the geochemical perspective:
1248 *Annual Review of Earth and Planetary Sciences*, v. 38, p. 133-160.
- 1249 Willbold, M., Stracke, A., 2010, Formation of enriched mantle components by recycling of upper
1250 and lower continental crust: *Chemical Geology*, v. 276, p. 188-197.
- 1251 Woodhead, J.D., and Devey, C.W., 1993, Geochemistry of the Pitcairn Seamounts. 1. Source
1252 character and temporal trends: *Earth and Planetary Science Letters*, v. 116, p. 81-99.
- 1253 Zindler, A., Hart, S., 1986, Chemical geodynamics: *Annual. Review of Earth and Planetary*
1254 *Sciences*, v. 14, p. 493-571.

1255

1256

1257 Figure captions:

1258 Fig. 1: (a) T-P simplified scheme of the classical view of Earth's shallow interior (modified from
1259 McKenzie and Bickle, 1988). Two geotherms for Archaean shield and old oceanic basin are
1260 shown. Dotted line indicates the solidus temperature (the temperature at which the first melt
1261 appears) for a pyrolite system. Pyrolite is an hypothetical chemical composition obtained by
1262 adding three parts by mass of depleted peridotite (dunite) + 1 part of tholeiitic basalt (Ringwood,
1263 1979). To the left of the solidus the temperature is too low for melting at any pressure. To the left
1264 of the solidus some melt is present. According to these geotherms, no melt should be present in
1265 the upper mantle. Dashed line indicates the adiabatic gradient, i.e., the temperature decrease per
1266 km of a solid rock. Partial melt can occur in the following cases: 1) the solid mantle adiabatically
1267 upwells (e.g., as a passive upflow following Anderson and Natland, 2014); 2) a temperature
1268 anomaly, e.g., from the deep mantle or 3), as follows. Mantle potential temperature (T_p) is a
1269 concept proposed by McKenzie and Bickle (1988) and corresponds to the temperature of magma
1270 at the Earth's surface. According to McKenzie and Bickle (1988) MORB T_p is slightly less than
1271 1300°C. (b) T-P simplified scheme of Earth's mantle. The thick line (1) schematically represents
1272 the classically accepted geotherm with two thermal boundary layers characterized by
1273 superadiabatic regimes, one close to the surface and the other at the top of the core, with the bulk

1274 of the mantle characterized by an adiabatic geotherm. The thin line (2) is one possible geotherm
1275 (Schubert et al., 2009) characterized by superadiabatic and subadiabatic geotherms and no
1276 adiabatic gradients. In the first scheme the maximum T is reached at the base of the lithosphere
1277 (~90-100 km in oceanic basins), with T_p as high as ~1300°C. Deeper mantle is hotter because
1278 self-compressed, but when brought to the Earth's surface it is characterized by the same T_p
1279 (~1300°C) as sub-lithospheric mantle. This temperature is considered to be ambient mantle T_p ,
1280 and recorded by MORB (e.g., McKenzie and Bickle, 1988). The most important differences
1281 between the two type of geotherms are: a) the maximum T_p of geotherm (1) is lower than that of
1282 geotherm (2); b) the maximum T_p of geotherm (1) is reached at shallower depths than geotherm
1283 (2); c) after the thermal bump at ~200 km the T_p in geotherm (2) decreases with depth while the
1284 T_p in geotherm (1) remains constant for nearly the entire mantle; d) D" in geotherm (1) is
1285 characterized by higher T_p than the entire mantle, while in geotherm (2) much of D" is
1286 characterized by lower T_p . The dashed lines represent the adiabatic upwelling of two samples of
1287 the lowermost mantle starting at temperatures compatible with geotherm (1) (star) and geotherm
1288 (2) (square). In the first case, which represents the classical mantle plume scheme, upwelling of
1289 solid mantle from D" is characterized by higher T_p , recorded in high T_p magma (inferred on the
1290 basis of high Mg/Fe ratios). In the second case (the fluid-dynamically and internally heated
1291 compatible model) upwelling of solid mantle from D" is characterized by lower T_p . The highest
1292 measurable T_p in this case is associated with mantle corresponding to the LLAMA mantle of
1293 Anderson (2011), around 200-250 km depth, corresponding to the worldwide, well-defined Low
1294 Velocity Zone (LVZ). A-B-C-D on the right of the figure represent the original seismological
1295 zones into which the Earth was divided (modified from Anderson, 2011).

1296

1297 Fig. 2: Schematic evolution of the $^{87}\text{Sr}/^{86}\text{Sr}$ isotopic ratio with time. ^{87}Sr is continuously produced
1298 by ^{87}Rb decay, while ^{86}Sr is the stable Strontium isotope. As a consequence $^{87}\text{Sr}/^{86}\text{Sr}$
1299 continuously increases with time. Partial melting has the effect of increasing the isotopic ratio
1300 rate in the melt and reducing it in the solid residuum.

1301

1302 Fig. 3: Rare Earth Elements (REE) normalized to primitive mantle estimates. The two curved lines
1303 indicate simplified patterns of partial melts and mantle solid residua after anatexis. The
1304 incompatibility of an element is its tendency to partition into the melt phase. Partial melts of a

1305 primitive mantle source are characterized by relatively high Nd/Sm ratios, while mantle residua
1306 are characterized by low Nd/Sm. With ageing these elemental ratios will evolve towards low
1307 $^{143}\text{Nd}/^{144}\text{Nd}$ and high $^{143}\text{Nd}/^{144}\text{Nd}$, respectively.

1308

1309 Fig. 4: Schematic $^{143}\text{Nd}/^{144}\text{Nd}$ vs. $^{87}\text{Sr}/^{86}\text{Sr}$ isotopic diagram reporting Bulk Silicate Earth (BSE)
1310 and Chondritic Uniform Reservoir (ChUR), which should represent the total average $^{87}\text{Sr}/^{86}\text{Sr}$
1311 and $^{143}\text{Nd}/^{144}\text{Nd}$ isotopic composition of the Earth. Starting from the initial composition, partial
1312 melting produces isotopic differentiation into depleted (<BSE and >ChUR) and enriched fields
1313 (>BSE and <ChUR) compositions.

1314

1315 Fig. 5: (a) $^{143}\text{Nd}/^{144}\text{Nd}$ vs. $^{87}\text{Sr}/^{86}\text{Sr}$ isotopic diagram for oceanic basalts. The background yellow
1316 strip is referred to the Sr-Nd isotopic mantle array. DMM = Depleted MORB Mantle; HiMu =
1317 High-Mu, where $\text{Mu} = \mu = ^{238}\text{U}/^{204}\text{Pb}$; EMI = Enriched Mantle Type I; EMII = Enriched Mantle
1318 Type II (from Stracke, 2012). (b) $^{143}\text{Nd}/^{144}\text{Nd}$ vs. $^{87}\text{Sr}/^{86}\text{Sr}$ isotopic diagram for continental rocks
1319 from the circum-Mediterranean area (Lustrino and Wilson, 2007; Lustrino, 2011). In both cases
1320 all the isotopic compositions can be defined in terms of relative abundance of four main
1321 components, similar to computer printers where all the possible colors are produced using four
1322 ink cartridges (black, yellow, magenta, blue).

1323

1324 Fig. 6: (a) $^{207}\text{Pb}/^{204}\text{Pb}$ vs. $^{206}\text{Pb}/^{204}\text{Pb}$ isotopic diagram showing the hypothetical evolution of the
1325 Earth system starting at 4.56 Gyr with primordial (solar) $^{207}\text{Pb}/^{204}\text{Pb} = 10.29$ and $^{206}\text{Pb}/^{204}\text{Pb} =$
1326 9.31 , evolving with different μ values. Model lower continental crust from Bolhar et al. (2007).
1327 Lower and upper continental crust fields from references reported in Lustrino (2005) and Bolhar
1328 et al. (2007). References for oceanic basalt field are from Stracke (2012). (b) $^{207}\text{Pb}/^{204}\text{Pb}$ vs.
1329 $^{206}\text{Pb}/^{204}\text{Pb}$ isotopic diagram illustrating the effect of partial melt extraction (producing melts M1
1330 and M2 and solid residua R1 and R2).

1331

1332 Fig. 7: (a) $^{207}\text{Pb}/^{204}\text{Pb}$ vs. $^{206}\text{Pb}/^{204}\text{Pb}$ isotopic diagram for oceanic basalts (references in Stracke,
1333 2012). Worth noting is the nearly complete overlap of MORB with OIB and the position to the
1334 right of the Geochron of nearly all the compositions. Also in this case, the Pb isotopic ratios of
1335 oceanic basalts can be defined in terms of only four end-members (the isotopic colors of the

1336 mantle printer). NHRL = Northern Hemisphere Reference Line (Hart, 1984) represents the
1337 average Pb isotopic composition of the Northern Hemisphere oceanic basalts. The vertical shift
1338 (negative or positive) from this line is defined by the parameter $\Delta 7/4\text{Pb}$. (b) $^{207}\text{Pb}/^{204}\text{Pb}$ vs.
1339 $^{206}\text{Pb}/^{204}\text{Pb}$ isotopic diagram for continental intra-plate volcanic rocks from the circum-
1340 Mediterranean area. References in Lustrino and Wilson (2007) and Lustrino (2011). The
1341 complete list of the analyses (>8000 rocks) is available on request to the first author.

1342

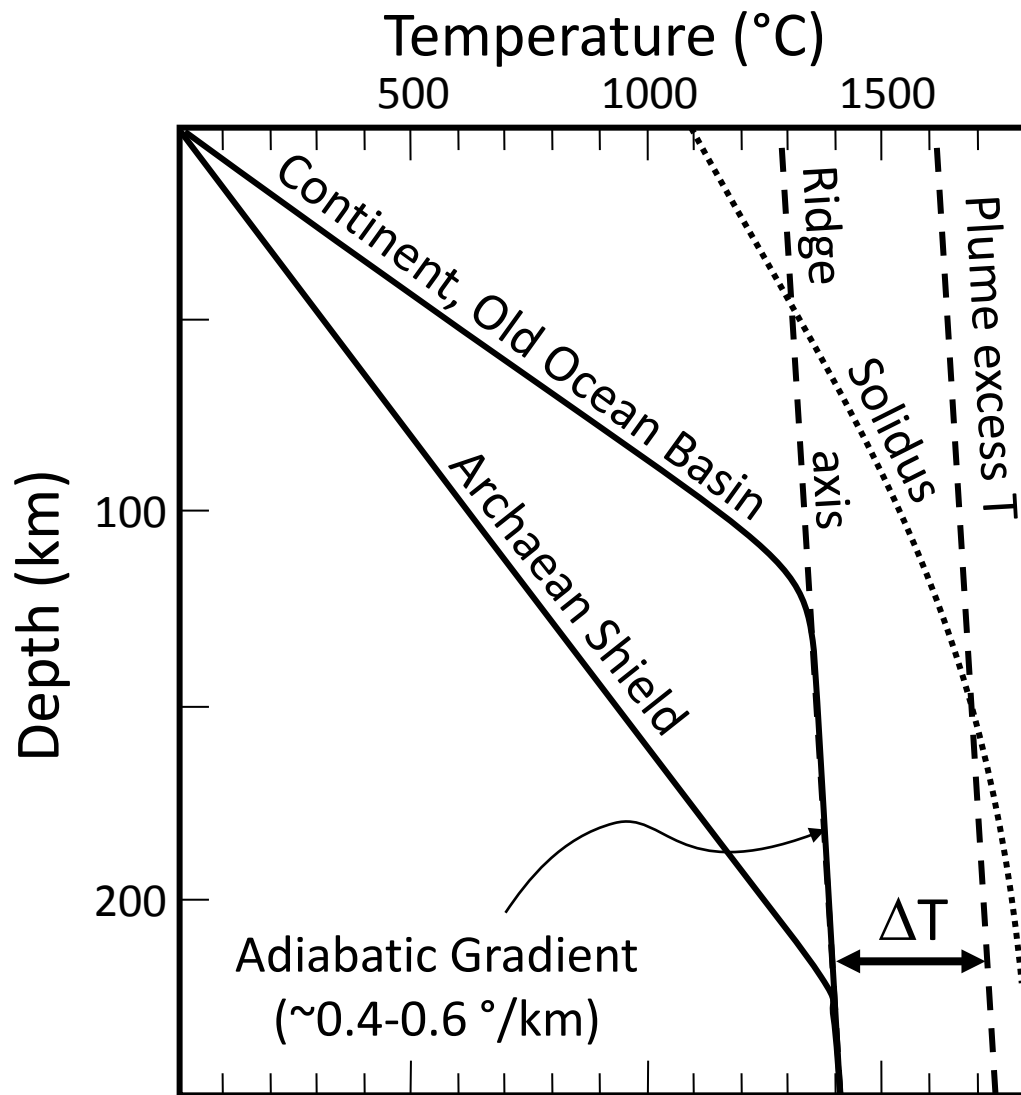
1343 Fig. 8: (a) Classical interpretation of isotopic evolution of $^3\text{He}/^4\text{He}$ system with age. The $^3\text{He}/^4\text{He}$
1344 ratio decreases continuously because of progressive ^3He escape and ^4He production by Th-U
1345 decay into stable Pb isotopes. An undegassed Earth (i.e., primitive mantle composition) would
1346 today be characterized by $^3\text{He}/^4\text{He}$ around 50 R/Ra (black dot 1). R is the isotopic ratio measured
1347 in the rock and Ra is the same ratio measured in the present-day atmosphere. D is the bulk
1348 distribution coefficient in the melting assemblage and quantitatively indicates the tendency of an
1349 element to remain into the solid (high D, high compatibility) or to preferentially partition into the
1350 melt (low D, high incompatibility). According to this view, He is more incompatible than Th+U
1351 during partial melting, resulting in a $^3\text{He}/(\text{Th}+\text{U})$ -poor mantle residuum (black dot 2). The melt
1352 will experience substantial degassing, resulting in strong ^3He depletion (dashed line). (b)
1353 alternative model of $^3\text{He}/^4\text{He}$ isotopic evolution, assuming stronger incompatibility of Th+U
1354 compared with He. In this case the solid residuum would be characterized by higher $^3\text{He}/(\text{Th}+\text{U})$,
1355 leading to higher $^3\text{He}/^4\text{He}$ compared with undegassed melt. Modified from Parman et al. (2005).

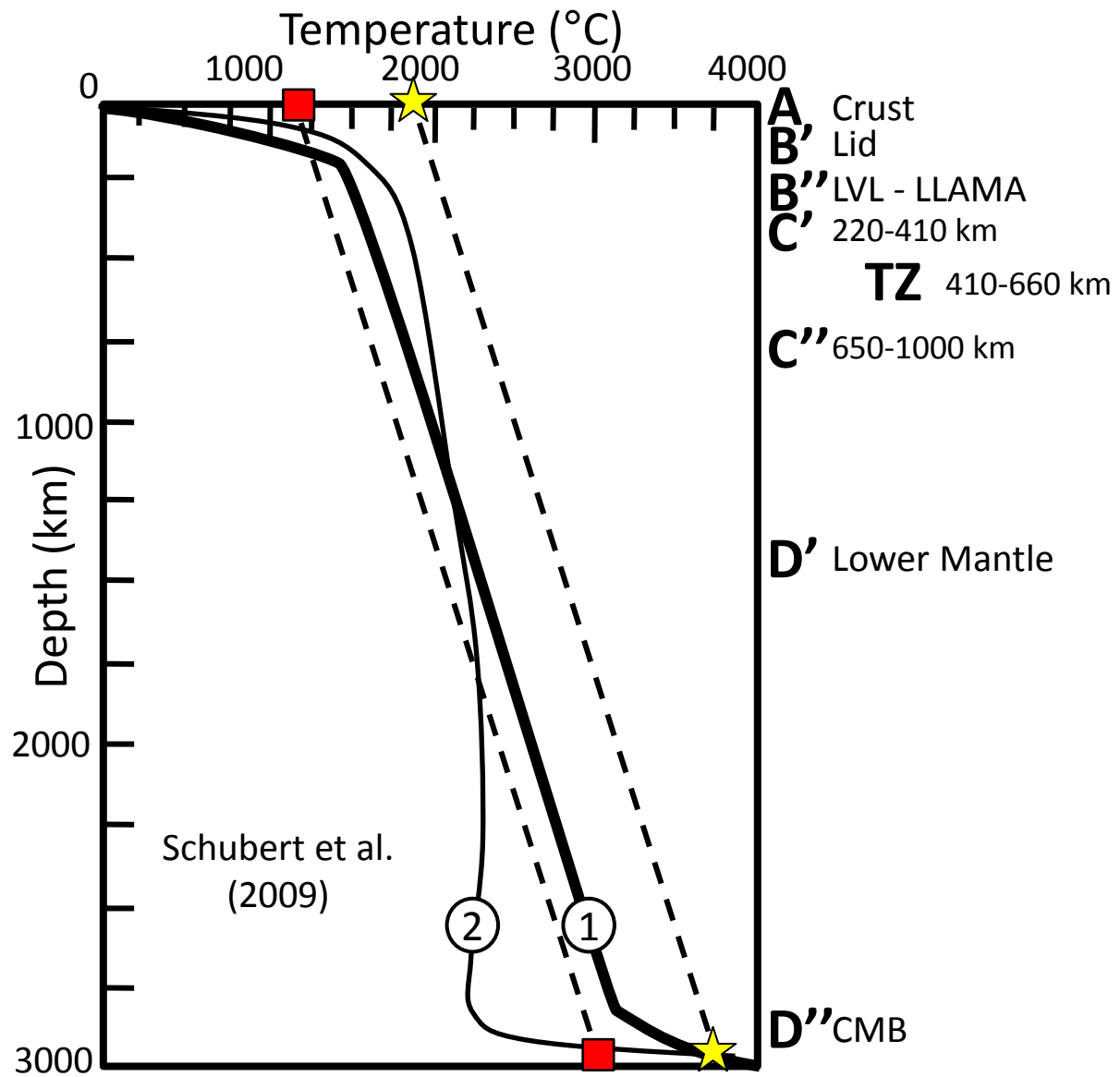
1356

1357 Table caption:

1358 Table 1: Main parent-daughter isotopic characteristics of the systematics discussed in the text. The
1359 column "%" reports the mass abundance of that isotope compared to the remaining isotopic
1360 masses.

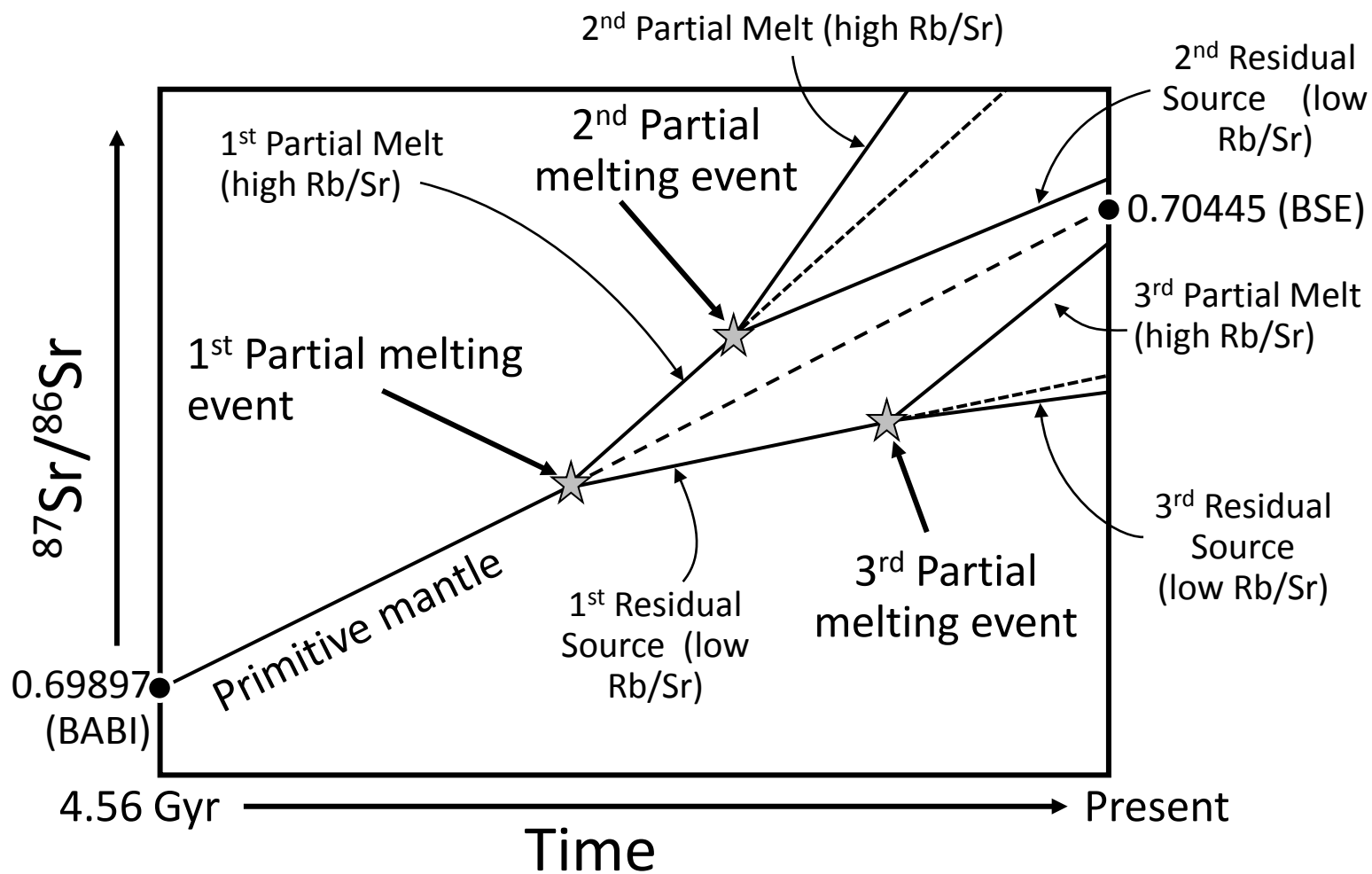
1361

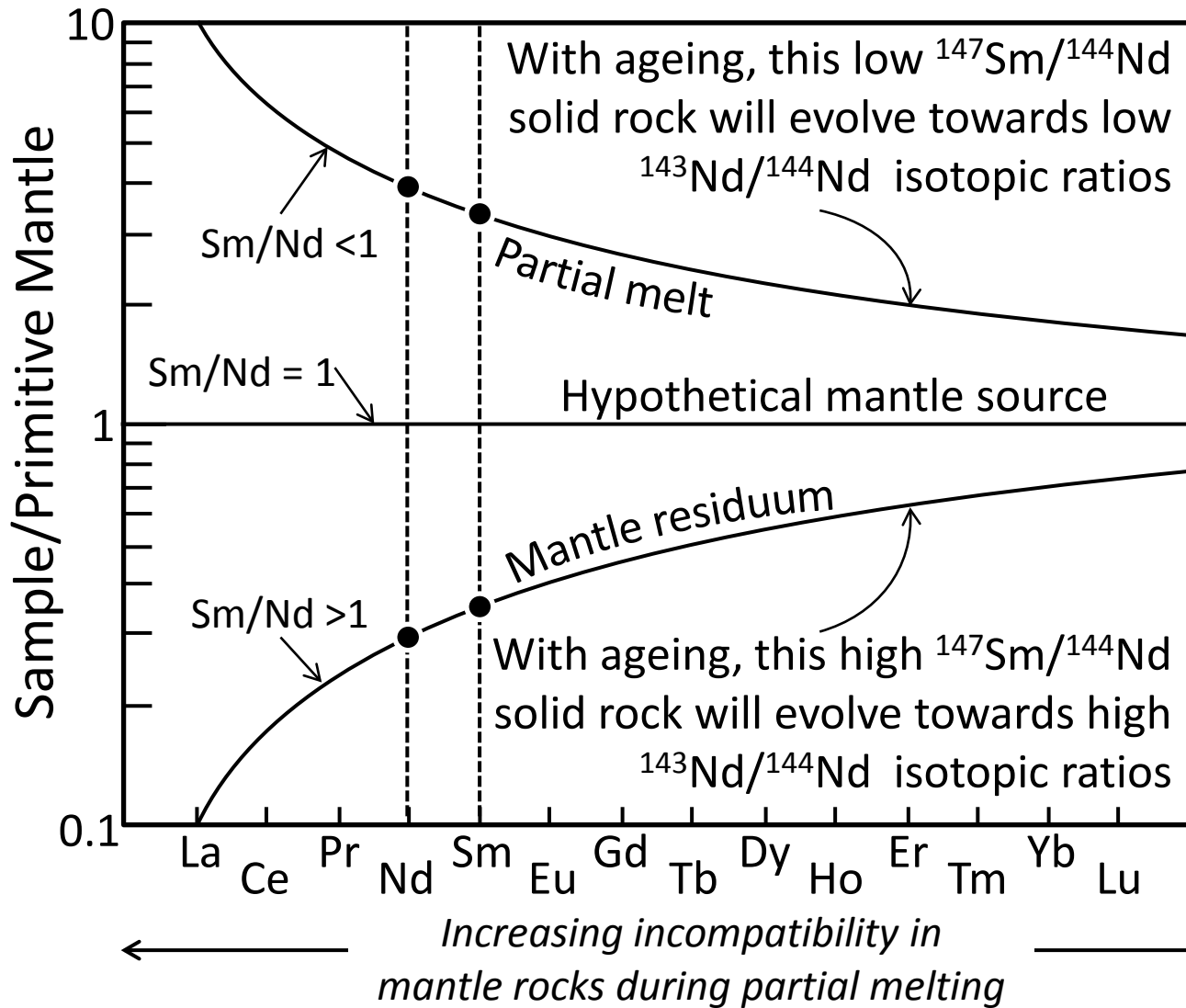




Lustrino and Anderson

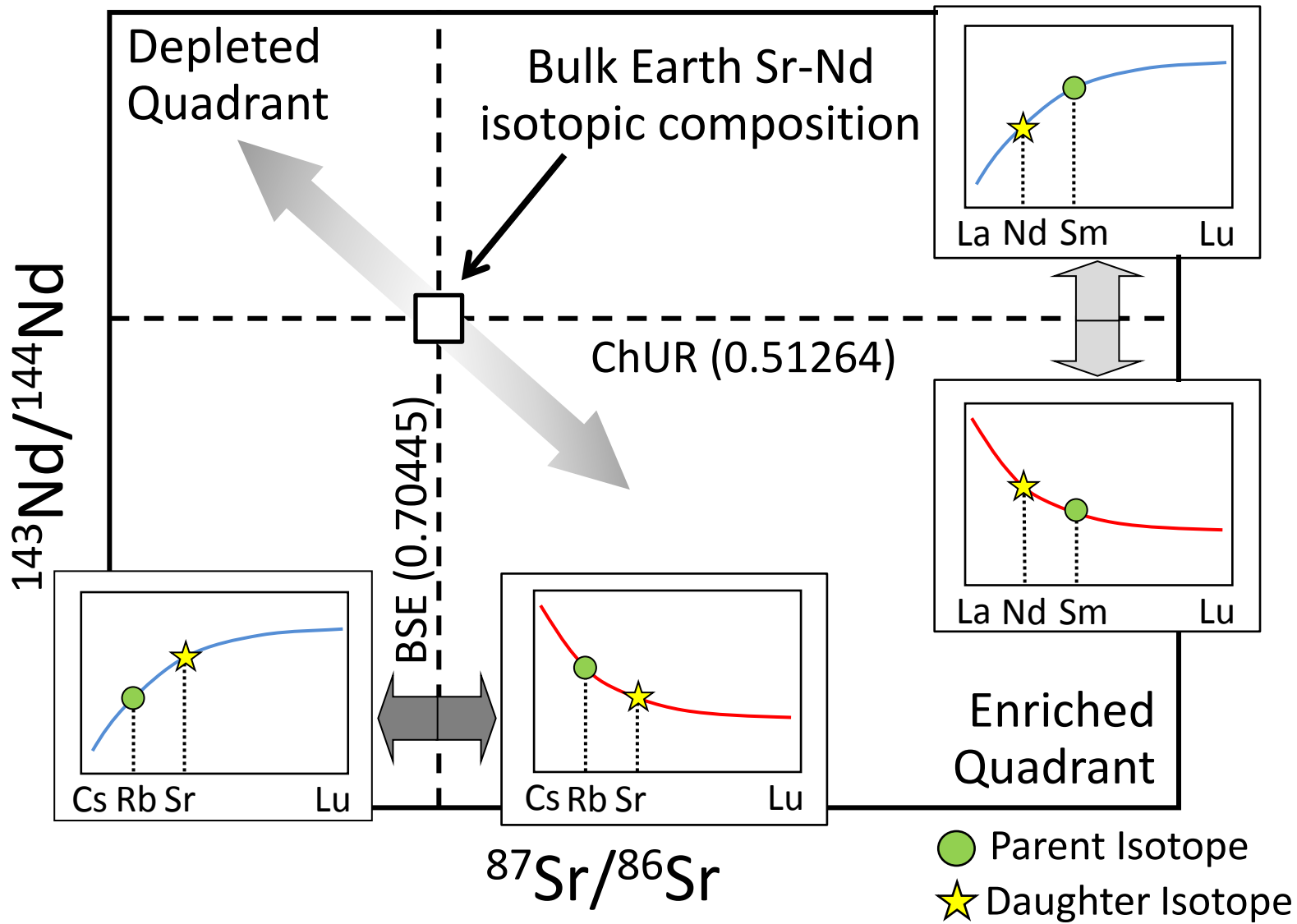
Fig. 1b

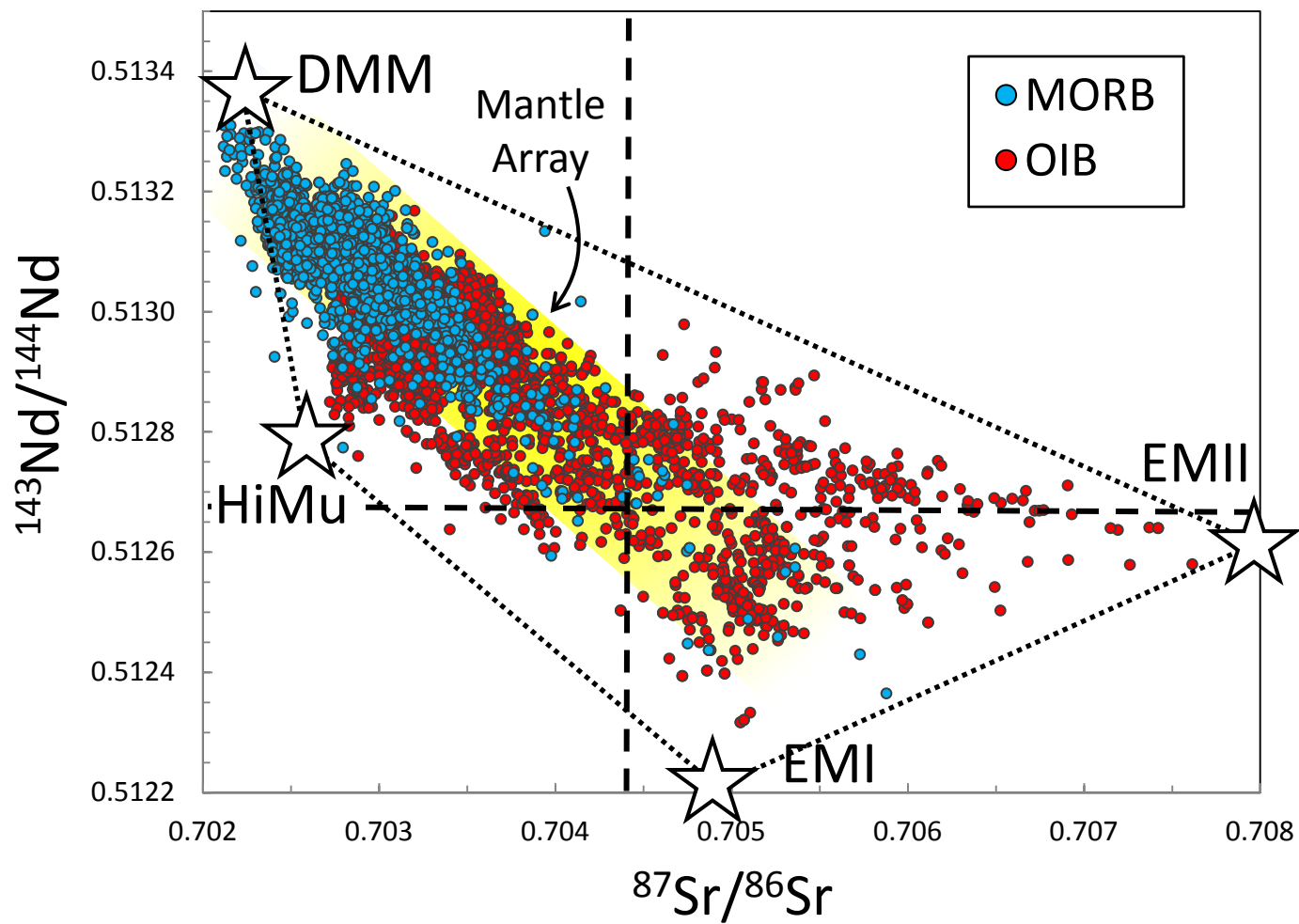




Lustrino and Anderson

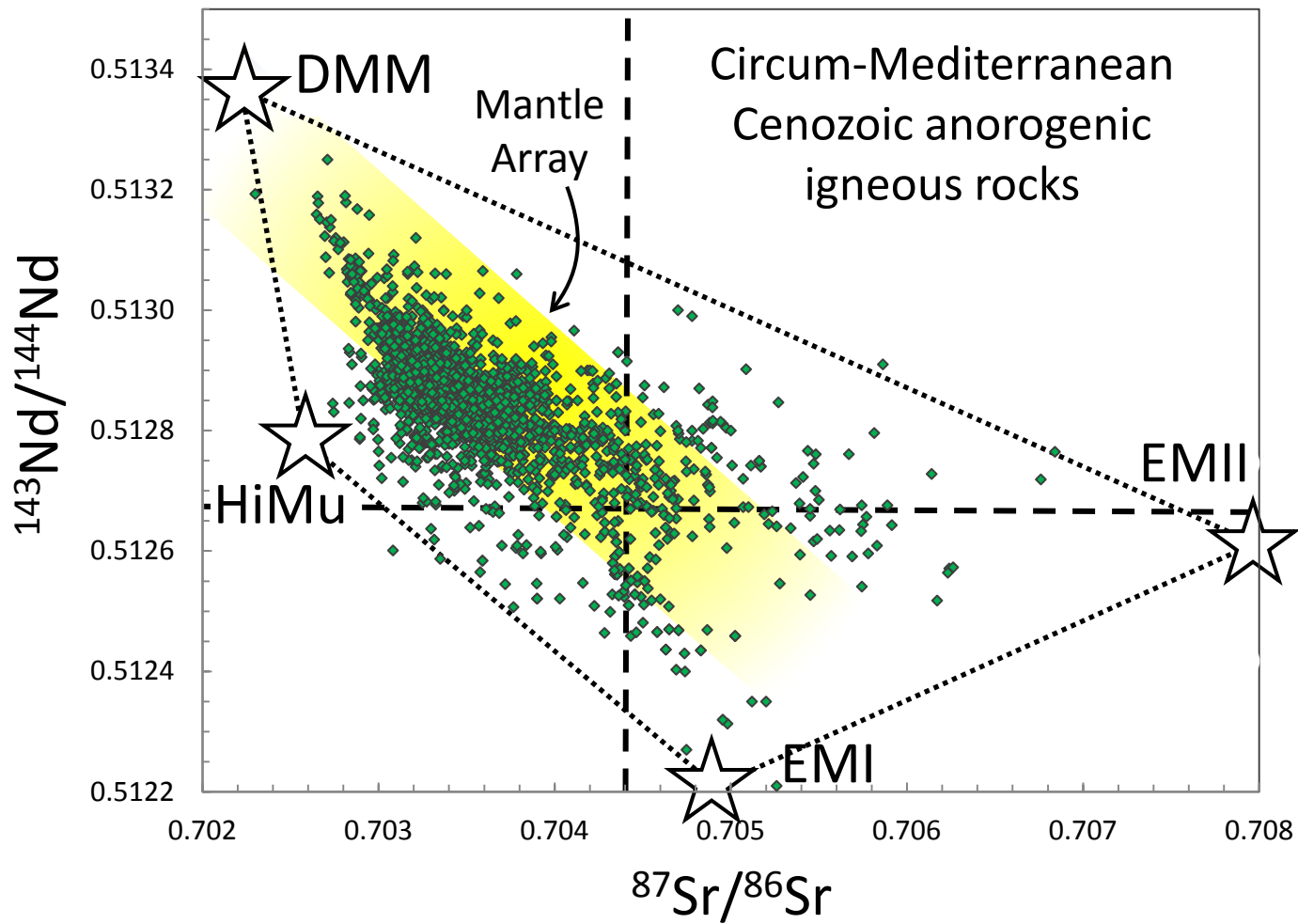
Fig. 3





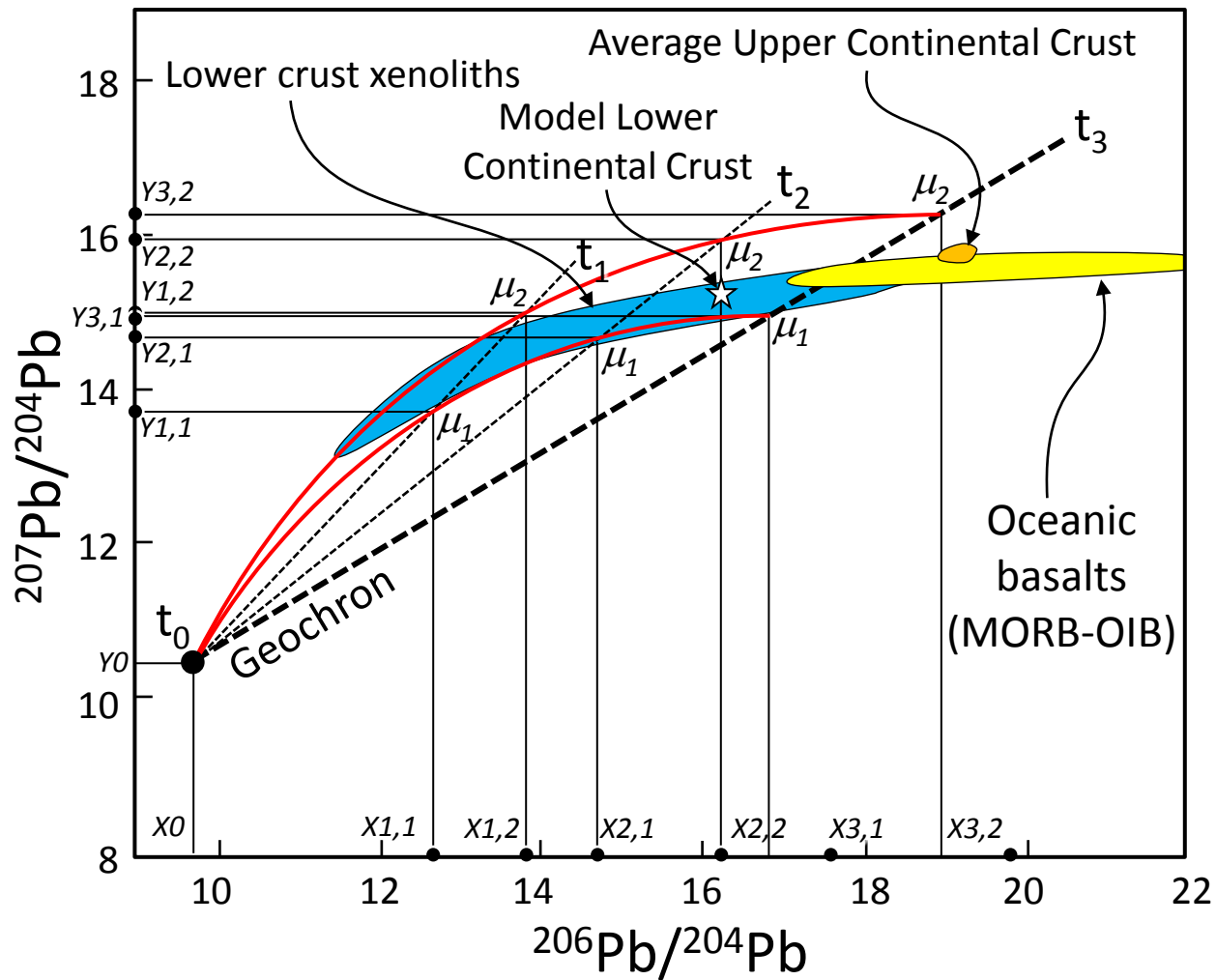
Lustrino and Anderson

Fig. 5a



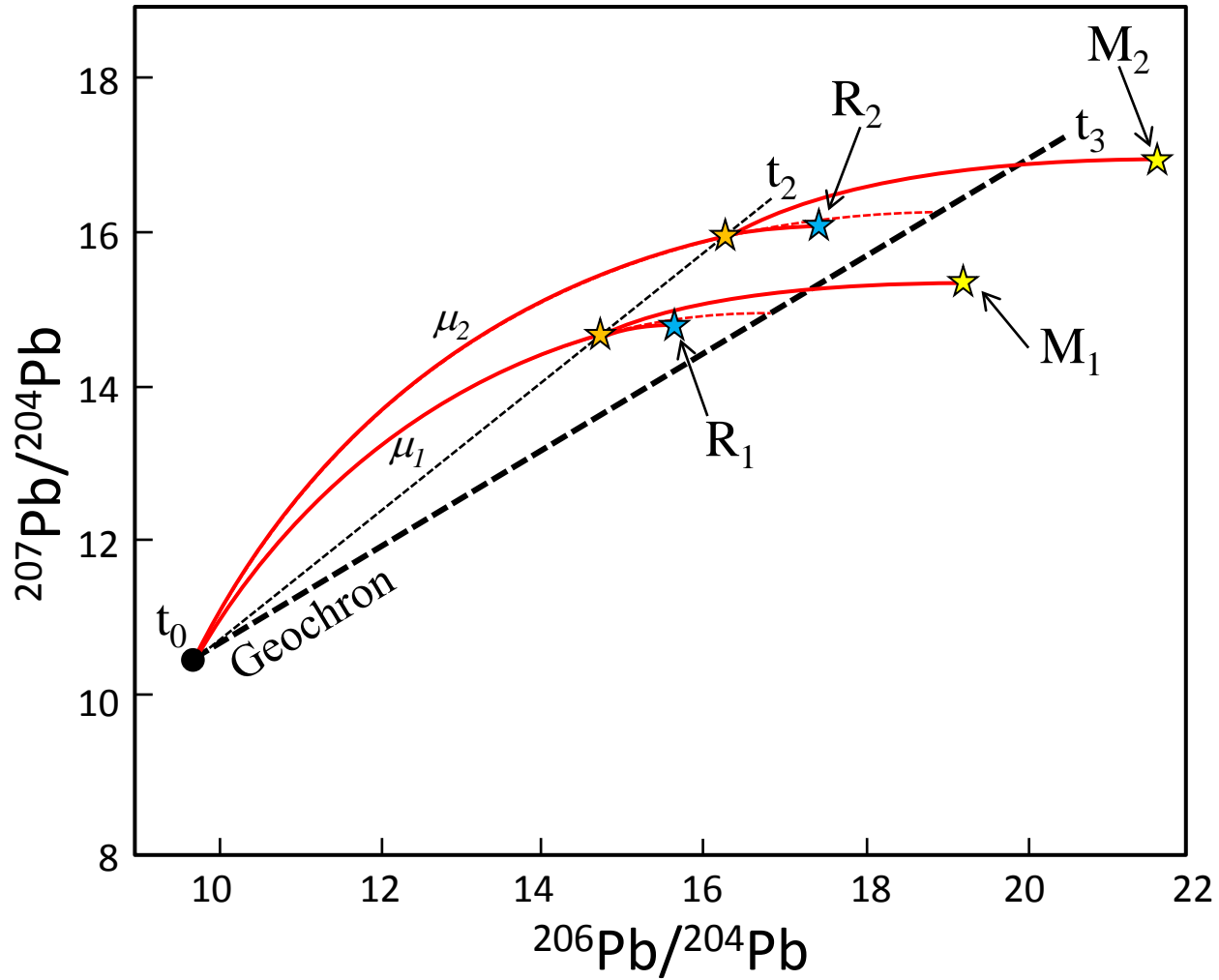
Lustrino and Anderson

Fig. 5b



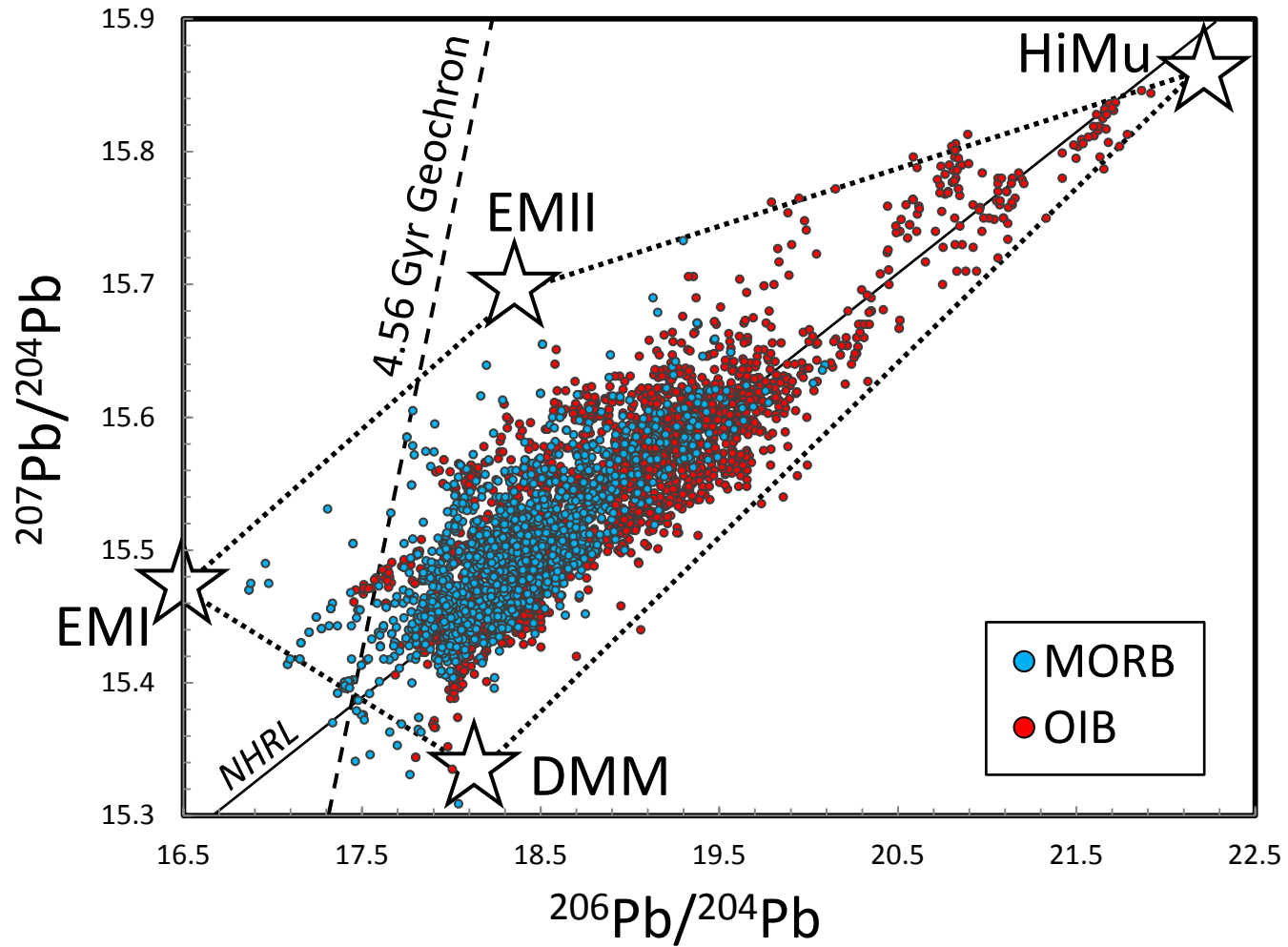
Lustrino and Anderson

Fig. 6a



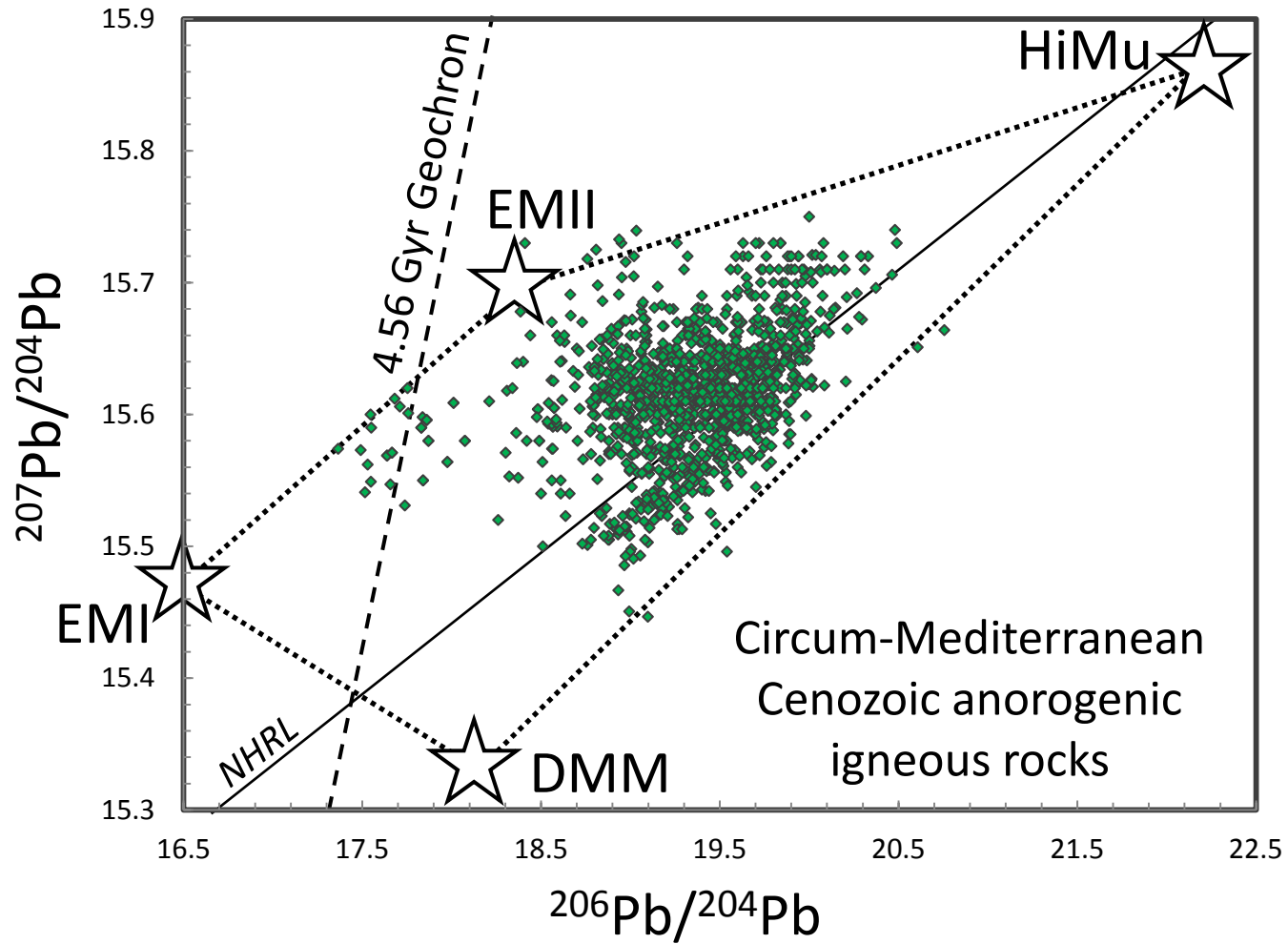
Lustrino and Anderson

Fig. 6b



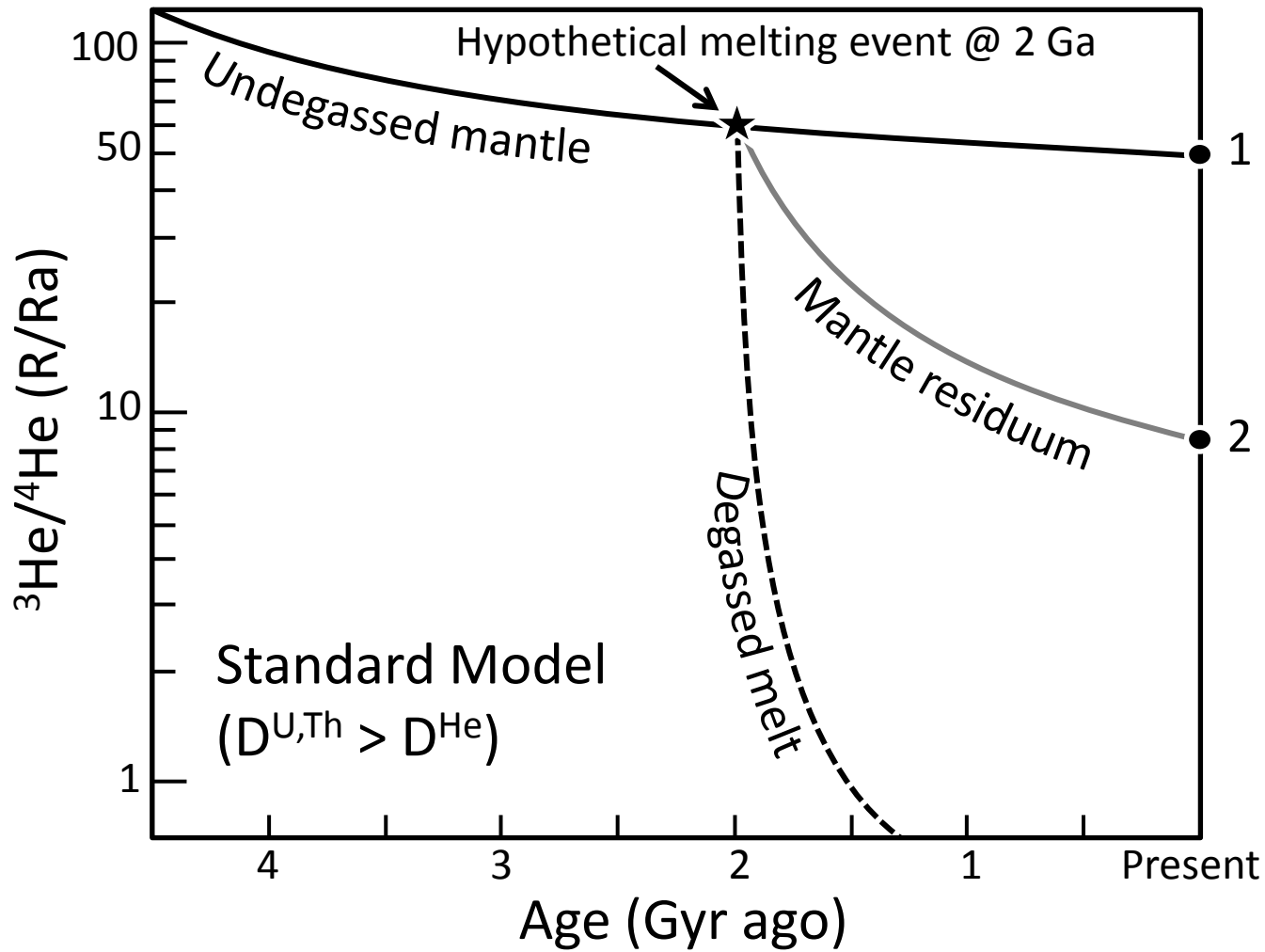
Lustrino and Anderson

Fig. 7a



Lustrino and Anderson

Fig. 7b



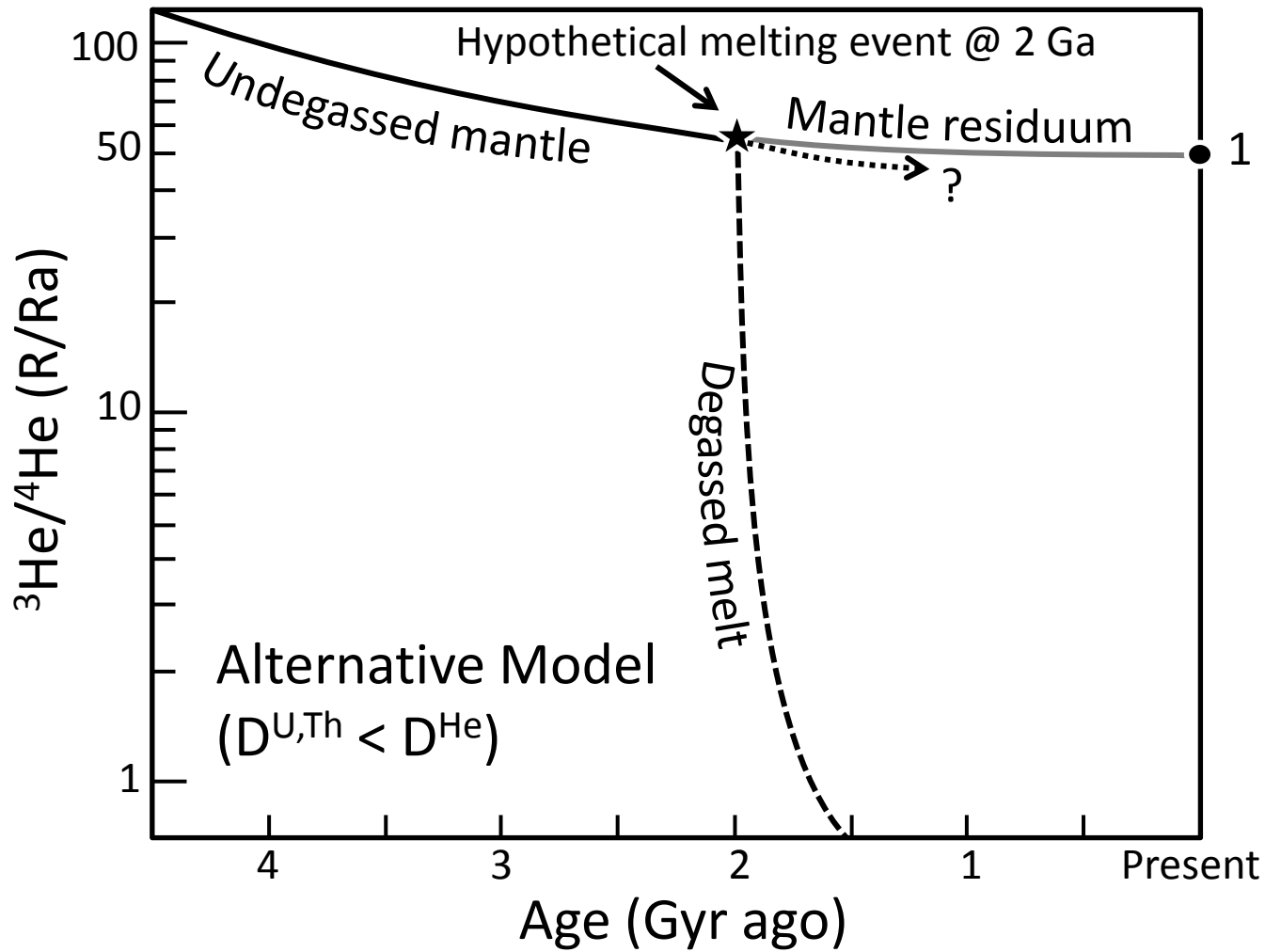


Table 1
Lustrino and Anderson

Parent	%	Half-life	Daughter	Parent/Daughter Ratios		Isotopic ratios	
					Present-day	Initial	Present-day
⁸⁷ Rb	27.8	4.8*10 ¹⁰ yr	⁸⁷ Sr	⁸⁷ Rb/ ⁸⁷ Sr	~0.072	⁸⁷ Sr/ ⁸⁶ Sr	0.69897 0.70445
¹⁴⁷ Sm	15.0	1.06*10 ¹¹ yr	¹⁴³ Nd	¹⁴⁷ Sm/ ¹⁴³ Nd	~0.202	¹⁴³ Nd/ ¹⁴⁴ Nd	0.506687 0.51264
²³² Th	100	1.4*10 ¹⁰ yr	²⁰⁸ Pb	²³² Th/ ²⁰⁸ Pb	~36	²⁰⁶ Pb/ ²⁰⁴ Pb	9.31
²³⁵ U	0.72	7.07*10 ⁸ yr	²⁰⁷ Pb	²³⁵ U/ ²⁰⁷ Pb	~8.5	²⁰⁷ Pb/ ²⁰⁴ Pb	10.29
²³⁸ U	99.28	4.47*10 ⁹ yr	²⁰⁸ Pb	²³⁸ U/ ²⁰⁶ Pb	~0.06	²⁰⁸ Pb/ ²⁰⁴ Pb	29.48